Advanced filter design for extremely sensitive optical biosensors

Adane Samuel Gebretsadik

Promotor: prof. Peter Bienstman
Begeleider:

Masterproef ingediend tot het behalen van de academische graad van
Erasmus Mundus Master of Science in Photonics

Vakgroep Informatietechnologie
Voorzitter: prof. dr. ir. Daniël De Zutter
Faculteit Ingenieurswetenschappen
Academiejaar 2008-2009

UNIVERSITEIT GENT

Acknowledgement

This thesis work would have not been possible without the help of my supervisors Dr.ir. Bjorn Maes and ir. Tom Claes. Their continuous assessment and invaluable comments have helped me a lot. I would like to thank Prof. Peter Bienstman for his help and critical comments during our meeting. I would like to thank the European Union for sponsoring my research work. I would like also to thank the Photonics research group for providing me important idea and materials whenever I needed. My thank also goes to ir. Nebiyu Adello and Bekele Homa for their encouragement and fraternal advice.

Finally I want to thank my family and friends for their help next to God.

Abstract

We have proposed a parallel coupled ring resonator filter configuration for biosensing in the SOI platform. The structure has a very narrow transmission peak in the middle of a relatively broader dip if properly designed.

Both numerical and experimental analysis have been carried out to investigate the performance of our structure in terms of the two figures of merit of a biosensor (sensitivity and detection limit) and compared with an add-drop channel filter configuration.

Simulation results have shown that our device has the same effective refractive index sensitivity as a single ring structure. However, for a properly designed CTC distance between the two rings and coupler length, a coupled ring resonator with the same or different ring size has a detection limit almost by an order of magnitude less than that of a single ring resonator.

We have achieved a full width value about 30pm at the 90% of the peak transmission through our experiment. This is in good agreement with the theoretical result.

Advanced Filter Design for Extremely Sensitive Optical Biosensors

Adane Samuel Gebretsadik

Promoters: Prof. Peter Bienstman, Dr. Ir. Björn Maes
Supervisor: Ir. Tom Claes

Abstract: **A parallel coupled ring resonator based on the SOI platform has been designed, fabricated, and characterized for bulk refractive index change and biomolecular detection. A full width at 90% of the transmission peak value of about 30pm has been achieved experimentally. The measurements agree well with the simulation results.**

I. INTRODUCTION

Optical biosensors have attracted a vast amount of attention in all spectrums of science such as Biology, Chemistry, and Physics. This is due to the fact that rapid and simple sensing and detection of bioanalytes are of huge significance for environmental monitoring, food safety, and diagnostic applications [1-3].

A key component in optical biosensors is a filter which actually determines the detection limit and performance of the overall sensing device. An optical filter that has emerged in the last few years is a microring resonator [1, 2]. Such filters for biosensing purpose can be fabricated based on the Silicon-On-Insulator (SOI) platform using standard CMOS processing which makes possible cheap mass production, integration with electronics, and an array of thousands of devices can be integrated to detect different types of molecules at the same time. SOI also results in a very high index contrast so that a highly miniaturized optical device with fairly good quality can be fabricated [3].

Recent investigations [9] have shown that parallel coupled microring resonators exhibit a very sharp transmission spectrum and could be achieved quality factor of about 11800. Due to the high Q-value or narrow transmission peak they intrinsically exhibit, it has been proposed that this system is applicable for slowing down light significantly so that a high performance optical buffer can be realized. The big advantage observed in such systems is that the highest optical delay is associated with the Fabry-Perot mode having the highest power transmission. This actually circumvents the tradeoff between transmission and delay that, for example, photonic crystals face [10]

In this thesis, we have proposed a parallel coupled microring resonators based on SOI for both bulk refractive index change detection and biosensing purpose. Due to the narrow and symmetric transmission spectrum they have, it is evident that the detection limit of the sensor circuit will be extremely low. The fact that our device is fabricated using CMOS technology, deep-UV lithography, in particular also enables us to take advantage of the cheap mass production, high throughput and easy integration with electronics.

II. A PARALLEL COUPLED RING RESONATOR

Figure-1(right) shows a parallel couple ring resonator filter configuration. The input light coming from the source will pass directly to the output port if the two rings are out of resonance. If only one of the rings is at resonance, the light from the source coupled to this ring passes through the drop port. Thus, the transmission spectrum shows a dip like a single ring resonator system. On the other hand, if both rings are at resonance, the input light will not be coupled directly to the second waveguide. Rather, for an optimum center-to-center (CTC) distance between the rings, the light from the source is coupled to the second ring. In this case, the two rings act like a mirror reflecting the light from one waveguide to the other between the two rings [10]. Thus, light is coupled into both ring resonators and they form a Fabry-Perot (FP)-like cavity with light traveling in the direction of the arrows indicated in Figure 1-1.

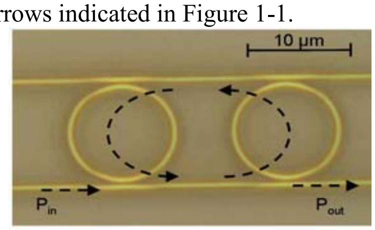

Figure 1-1 Microscopy image of a parallel coupled ring resonator

Adane Samuel

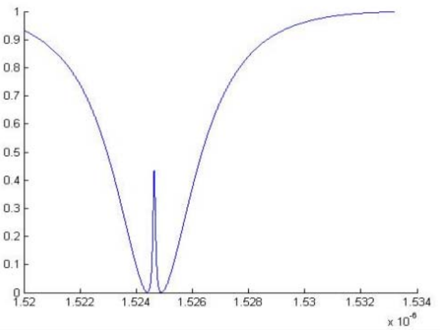

Figure 1-2 Transmission spectrum of a coupled ring resonator with 0.4nm detuning

The transmission spectrum of such a filter configuration strongly depends on the geometry of the device [9, 10]. Both experimental and simulation results have shown that, at resonance, a small detuning in resonance between the two rings results in a very narrow and symmetric transmission peak. The width of the transmission spectrum is also a strong function of the center-to-center (CTC) distance between the rings as the spacing between the two mirrors of a Fabry-Perot interferometer influences its transmission properties. Moreover, the coupling loss has also a remarkable influence on the width of the transmission peak since it is directly related to the Q-factor of the resonator structure. The Q-factor and the 3dB width of a resonator structure are mathematically related as $Q=\lambda/\Delta\lambda$.

III. SIMULATION RESULTS

Sensitivity

Sensitivity is the measure of ''how much'' the resonance wavelength of the resonator shifts for a given change in the effective refractive index felt by the field expanding from the core to the upper cladding [5]. We have simulated the sensitivity of both a coupled ring resonator with the same and different ring size and compared their performances with a single ring resonator. Our simulation results have shown that a parallel coupled ring resonator with the same or different ring resonator have the same effective refractive index sensitivity as an add-drop channel filter configuration. This is due to the fact that the resonance wavelengths of the two rings of a coupled ring resonator shift by the same amount for a given amount of effective refractive index change resulting in the same performance as an add-drop channel filter configuration.

FWHM

The width of the transmission peak of a resonator structure determines the smallest resonance wavelength shift one can detect and thus determines the smallest amount of biomolecules that the sensor can detect. The narrower the peak width, the lower the detection limit of the biosensing device. As we described earlier, the CTC distance between the rings and the power coupling ratio to the ring resonator strongly influence the transmission peak width of a coupled ring resonator. Our simulation results have shown that the full width at half maximum (FWHM) for a coupled ring resonator with the same or different ring sizes is less almost by an order of magnitude than that of a single ring resonator. Moreover, a coupled ring resonator with the same ring size performs better than with different ring size.

The CTC distance and the coupling loss of a coupled ring resonator have been optimized for the best performance of our ring structure in terms of its detection limit. Due to the asymmetric nature of the transmission peak of a coupled ring resonator with the same ring size, the peak width at the 90% of the transmission peak has been simulated. At 90% of the transmission peak, a FW of 31picometer (Figure 1-3) has been found for 0.4nm detuning in resonance and 6pm (not shown) for similar ring size coupled ring resonator.

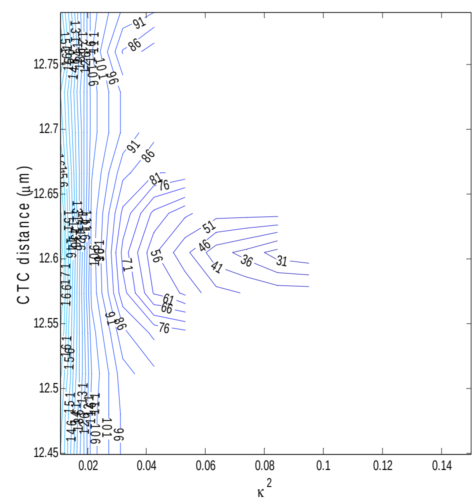

Figure 1-3 FW (pm) at 90% of the transmission peak with 0.4nm resonance detuning and 2.4dB/cm loss

IV. DESIGN

The design consists of two racetrack shaped rings having bend radius of 5µm. Both the straight and curved waveguides are designed to be 450nm wide and 220nm thick. The gap between the bus and the straight segment of the racetrack is taken to be 180nm. The length of the coupler has been optimized in such a way that 30% of the total power can be coupled to the ring resonator to achieve a Q-factor value of 1000 for each ring resonator. The CTC distance between the rings have been swept and the size of the rings has been left the same assuming a detuning of 0.5nm can be achieved from fabrication error.

V. FABRICATION AND EXPERIMENTAL RESULTS

Fabrication

Our structures have been fabricated using CMOS technology at IMEC, Leuven. The waveguide structures are patterned on SOI wafer using 193nm deep UV optical lithography. The structures are then created by etching the 220nm thick top silicon layer on the wafer. The silicon layer is isolated from the substrate by 2µm thick bottom SiO_2 cladding. Since our structures are formed in the SOI platform, their dimension can be highly miniaturized. Owing to the high refractive index contrast, the waveguide core is largely reduced in size and can be made single mode. In addition, total internal reflection guiding is guaranteed for very small bend radii.

Setup and Measurement results

Input light from a tunable laser is vertically coupled to the SOI coupled ring structure. The laser has tuning resolution of about 5pm and it is tunable in 1500-1640nm wavelength range. Coupling from optical fiber to the waveguide structures is achieved with grating couplers. The output fiber coupler is directly connected to the photodetector so that the reflected or transmitted light through our structure can be measured.

The experimental measurements have been carried out with water and air top cladding. As we can see from Figure 1-4, an EIT like transparency has been realized from our structures.

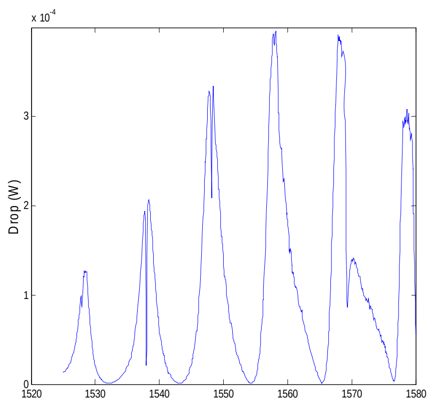

Figure 1-4 Output power at the drop port for air cladding with CTC 12.4824µm

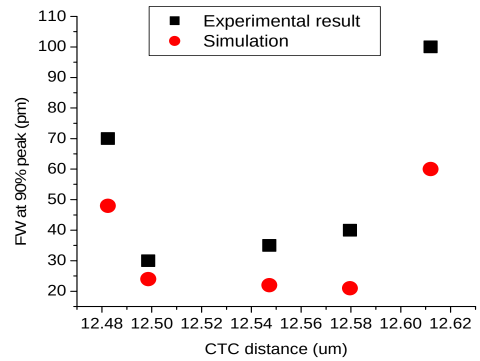

Figure 1-5 Full width at the 90% transmission peak for water cladding and κ^2=0.3

Figure 1-5 shows that a FW of 30pm at the 90% transmission peak has been found in good agreement with the theoretical result that predicts an optimum value of 20pm assuming 30% of the total power is coupled to the ring structure.

VI. CONCLUSION

It has been revealed that the transmission spectrum of our devices is indeed identical to the theoretical EIT like transparency with a narrow peak in a relatively broader dip. A coupled ring resonator with the same or different ring size has the same effective refractive index sensitivity but has a detection limit of an order of magnitude less than that of an add-drop channel filter configuration. Both the experimental and simulation results have shown that there is an optimum full width at the 90% of the transmission peak with a fairly good agreement.

List of Acronyms

ASPIC	Advanced Simulation for Photonic and Integrated Circuit
CAD	Computer Aided Design
CMOS	Complementary Metal –oxide Semiconductor
CTC	Center-to-Center
EIT	Electromagnetic Induced Transparency
FP	Fabry-Perot
FSR	Free Spectral Range
FWHM	Full Width at Half
IMEC	Interuniversity Microelectronics Centre
Q	Quality Factor
RIU	Refractive Index Unit
Si	Silicon
SiO2	Silicon Oxide
SOI	Silicon -on - Insulator
SPR	Surface Plasmon Resonance
TE	Transverse Electric
TIR	Total Internal Reflection
TM	Transverse Magnetic
UV	Ultra Violet
WGM	Whispering Gallery Mode
WGD	Waveguide

List of Figures

Figure 1-1	Schematic diagram of a single ring resonator
Figure 1-2	Transmission spectrum of a single resonator on the drop port
Figure 1-3	Picture of a parallel coupled microring resonator
Figure 1-4	Transmission spectrum simulated for s=15.69µm, $\Delta\lambda$=0.4nm, Q_c=1000, and Q_{rad}=25000
Figure 1-5	Simulation result of Power transmission for parallel coupled ring resonators with size R=5um
Figure 2-1	Schematic diagram of an asymmetric slab waveguide
Figure 2-2	waveguide structure in SOI
Figure 2-3	Schematic diagram of a racetrack shaped ring resonator
Figure 2-4	Transmission of parallel coupled ring resonator a) for S=12.69um, b) for S=12.71um, c) for S=12.73um
Figure 2-5	ASPIC simulation result (left) for the transmission spectrum (right) for the sensitivity of a single resonator with loss
Figure 2-6	ASPIC simulation result for the sensitivity of a parallel coupled ring resonator with different ring size and without loss

Figure 2-7	FWHM swept over the coupling ratio
Figure 2-8	Full width at 90% of the transmission peak of a coupled ring resonator with detuning 0.4nm swept over the coupling ratio and the CTC distance betwen the rings.
Figure 2-9	FW at 90% of the transmission peak for a coupled ring resonator with the same ring size swept over the coupling ratio and the CTC distance betwen the rings.
Figure 3-1	Mask design for a coupled ring resonator
Figure 3-2	Fabrication process for nanophotonic structures in SOI using deep UV lithography
Figure 3-3 setup	Schematic diagram of the measurement
Figure 3-4	Output Power at the pass port with water cladding and CTC distance between rings 12.45μm
Figure 3-5	Output Power at the drop port with air cladding and CTC distance between rings 12.4824μm
Figure 3-6	Output Power at the drop port with water cladding and CTC distance between rings 12.45μm
Figure 3-7	Full width at the 90% transmission peak for water cladding and κ^2=0.3

Table of Contents

Chapter One…….1

1. Introduction………1

1.1 Motivation………*1*

1.2 Overview of Transmission Properties of Microring Resonators………………………………………………*4*

1.2.1 *Single ring resonator……………………………………………………………………………………………4*

1.2.2 *Parallel coupled microring resonators with different ring size……………………………………………6*

1.2.3 *Parallel coupled microring resonators with same ring size…………………………………………………8*

1.3 Basic Principles of Biosensing Based on SOI Microring Resonators……………………………………………9

1.4 General Idea of the Thesis……………………………………………………………………………………………10

Chapter Two……….11

2. Design………11

2.1 Theoretical Background of Optical Waveguides and Design……………………………………………………11

2.2 Coupler Design……13

2.3 ASPIC and Matlab Simulation Results…………………………………………………………………………16

2.3.1 Optimization Parameters…………………………………………………………………………………………17

2.3.1.1 *ASPIC simulation results for the sensitivity of single ring resonators…………………………………19*

2.3.1.2 *ASPIC simulation results for the sensitivity of a parallel coupled ring resonators with identical and different ring size*……………………………………………………………………………20

2.3.2 Influence of the device parameters on the peak width…………………………………………………22

2.3.3 Summary of the Chapter………………………………………………………………………………………26

Chapter Three…….27

3. Fabrication and Measurement Results……………………………………………………………………………27

3.1 Mask Design………27

3.2 Fabrication……29

3.3 Measurement………30

3.4 Measurement Results and Comparison with Theory……………………………………………………………32

3.4.1 Measurement Results……32
3.4.2 Comparison with theory……35
3.5 Summary of the Chapter……36
Chapter Four……38
4. Summary and Recommendations……38
4.1 Summary……38
4.2 Recommendations and Future plan……41
Bibliography……43

Chapter One

1. Introduction

1.1 Motivation

Optical biosensors have attracted a vast amount of attention in all spectrums of science such as Biology, Chemistry, and Physics. This is due to the fact that rapid and simple sensing and detection of bioanalytes are of huge significance for environmental monitoring, food safety, and diagnostic applications [1-3].

A key component in optical biosensors is a filter which actually determines the detection limit and performance of the overall sensing device. An optical filter that has emerged in the last few years is a microring resonator [1, 2]. Such filters for biosensing purpose can be fabricated based on the Silicon-On-Insulator (SOI) platform using standard CMOS processing which makes possible cheap mass production, integration with electronics, and an array of thousands of devices can be integrated to detect different types of molecules at the same time. SOI also results in a very high index contrast so that a highly miniaturized optical device with fairly good quality can be fabricated [3].

Microring resonators, in general, do not require a facet or gratings for their optical feedback and are, therefore, suitable for monolithic integration with other optical devices such as lasers or photodetectors. Moreover, a specific transmission spectrum can be designed by the use of multiple serial or parallel coupled ring resonators [4, 9]. One of the critical issues of the ring-resonators, however, is polarization sensitivity which limits their applications in fiber-optic related systems in which the polarization states of optical signals may change randomly over time.

The fundamental concept of guided wave biosensing is based on the effective index change of the mode due to a change in refractive index of the surrounding. Since light passes only once in a waveguide, relatively longer waveguides may be required in order for adequate interaction time between the evanescent light and the analyte (to be sensed) be achieved [5]. This actually put threshold sensing limit with such sensors. Nevertheless, in an optical ring resonator, light propagates in the form of whispering gallery modes (WGM), resulting from the total internal reflection of light along the curved surface. WGM is a surface mode which circulates along the resonator surface and interacts repeatedly with the analytes on its surface through WGM evanescent field [6].

For optical biosensors, sensitivity is fundamentally determined by how efficiently the electromagnetic field inside the core couples to biomolecules in contact with the sensor surface. The electric fields associated with propagating light or optical standing waves will tend to concentrate themselves into materials with higher refractive index or the core. Most optical biosensors contain a material or structure allowing electric fields to concentrate themselves at the surface of the sensor in contact with a liquid sample that has a refractive index higher than the surrounding material. Although the electric field may reside mostly within the core, the evanescent field extends out of the core and into the surrounding medium (typically water with $n = 1.33$) [5, 6].

Several integrated biosensors such as based on Surface Plasmon Polaritons (SPPs) [6], resonant cavities [7], and Interferometers [8] have been demonstrated. Where the former approach, SPP based biosensors, take advantage of the fact that a change in the refractive index due to the binding of analyte molecules to biomolecular recognition elements trapped on the metal surface results in a change in the propagation constant of SPPs. Like surface plasmon resonance sensors or grating coupler based sensors, the interferometric biosensor is an evanescent field sensor and therefore sensitive to changes in surface mass coverage so that a relatively large amount of analyte is needed [3, 8].

Recently, K. De Vos etal has proposed a single microring resonator based on SOI for the detection of a bulk refractive index change and label free biomolecular detection. It has been reported that a refractive index change of 10^{-5} and protein concentration below 10ng/ml could be detected in an area below $10\times10\mu m^2$. The concept of shift in resonance wavelength as the refractive index of the environment changes is used for sensing the change in bulk refractive index. To assess sensing of biomolecules with microring resonators, the well known avidin-biotin binding chemistry has been utilized. When a biotinylated solution is introduced to a surface functionalized with avidin, the molecular binding changes the effective index of the microcavity and gives rise to a shift in its resonant modes [2].

Recent investigations have shown that parallel coupled microring resonators exhibit a very sharp transmission spectrum and could be achieved quality factor of about 11800 [9]. Due to the high Q-value or narrow transmission they intrinsically exhibit, it has been proposed that this system is applicable for slowing down light significantly so that a high performance optical buffer can be realized. The big advantage observed in such systems is that the highest optical delay is associated with the Fabry-Perot mode having the highest power transmission. This actually circumvents the tradeoff between transmission and delay that, for example, photonic crystals face [10].

In this thesis, we have proposed a parallel coupled microring resonators based on SOI for both bulk refractive index change detection and biosensing purpose. Due to the narrow and symmetric transmission spectrum they have, it is evident that the detection limit of the sensor circuit will be extremely low. The fact that our device is fabricated using CMOS technology, deep-UV lithography, in particular also enables us to take advantage of the cheap mass production, high throughput and easy integration with electronics.

In addition, sensor arrays can easily be implemented using resonators since the basic sensing scheme itself is suitable to multiplexing. Sensing using such structures is manifested by a shift in resonance wavelength of the rings. Hence several such sensors working at separate resonances and designed for sensing various matters can easily be multiplexed [3, 20].

Working on telecom wavelengths for biosensing is advantageous since the standardized telecom facilities can be reused [3].

1.2 Overview of Transmission Properties of Microring Resonators

1.2.1 Single ring resonator

Ring resonators utilize an optical feedback allowing a travelling wave to interfere with itself. If a single ring is coupled to two straight waveguides as shown in figure 1, some amount of the input light is transferred to the output port at resonant wavelengths [4]. As demonstrated in figure 1, input light coupled through port 1 of one of the waveguides (WGD1), is transmitted directly to port 2 under non-resonance condition. At resonance, part of this input is transferred to the second waveguide (WGD2) and leaves through port 3. In a lossless cavity case, all the input power can be coupled to the output port. The strength of the coupling between the ring and the straight waveguides is a strong function of the center-to-center (CTC) distance between the straight and the curved waveguides with the minimum distance limited by the resolution of the fabrication technique implemented [11].

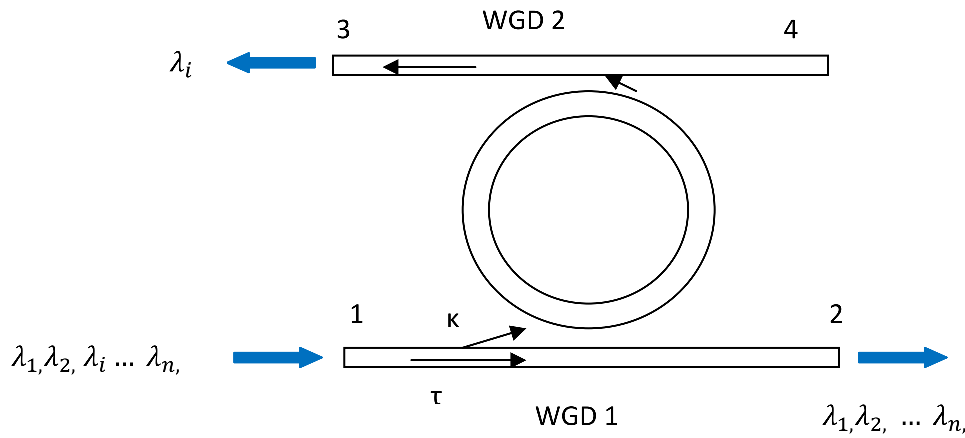

Figure 1-1 Schematic diagram of a single ring resonator

If one of the input wavelengths, $\boldsymbol{\lambda_i}$, satisfies the resonant condition, i.e.

$$2n_{eff}L = m\lambda_i, \tag{1.1}$$

then coupling of the wave with λ_i will be enhanced and all others will be suppressed so that only λ_i will be dropped from port 3 while the rest of the wavelengths will pass through port 2. Here n_{eff} is the effective index of the curved waveguide, L is the half-round trip length, and m is an integer. As a result, the transmission spectrum from the input to the drop port of a single-resonator looks a Lorentzian-like lineshape [12]. If the output power is measured through the drop port, the transmission spectrum will be a peak with some width. However, one will obtain a dip in the transmission spectrum if measured from the pass port.

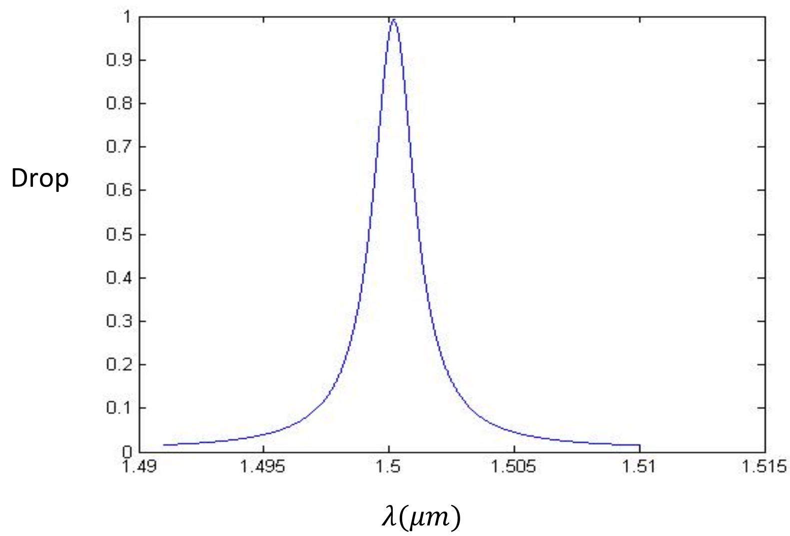

Figure 1-2 Transmission spectrum of a single resonator on the drop port

The key specifications or parameters evaluating the performance of these resonators are the free-spectral range (FSR), the quality-factor (Q), the transmission at resonance, and the extinction ratio. The major physical characteristics controlling these performance criteria are the size of the ring, the waveguide loss, and the input and output coupling ratios (analogous to the reflectivity of a Fabry–Perot resonator). Among the various types of losses, sidewall scattering loss, bending radiation loss, and substrate leakage loss are the dominant ones.

FSR is defined as the distance between two consecutive resonance wavelengths and is given by [12]

$$FSR = \frac{\lambda_i^2}{2n_g L} = \frac{\lambda_i^2}{n_g(2\pi R + 2L_c)} \tag{1.2}$$

Where R is the radius of the ring and L_c is the coupler length in case of a racetrack ring resonator. It should be noted that the FSR is inversely proportional to the size of the ring and hence the ring should be as small as possible to achieve a relatively high FSR value. Another resonator figure of merit is the Q-factor, which is a measure of the rate at which the energy of any resonant system decays, is defined as the ratio of the operating wavelength to the 3dB bandwidth of the transmission spectrum. After some rigorous mathematics, one can show that

$$Q = \frac{\tau A \pi (2L) n_g}{\lambda(1-\tau^2 A^2)} \tag{1.3}$$

where $\tau^2 = 1 - \kappa^2$ is the normalized coupling ratio in a lossless case representing the ratio of the power passing directly to the pass port with κ^2 being the power ratio coupled to the ring resonator, $A = e^{-\alpha L}$ is the amplitude over half the round trip with α being the total amplitude attenuation coefficient for each round trip. We note that the value of the Q-factor can be controlled by the size of the ring, external coupling, and internal losses. Since this parameter is inversely proportional to the 3dB width of the transmission peak, high Q-factor values correspond to very narrow spectral peaks. Therefore, the minimum detectable shift in resonance wavelength is determined by the Q-value of the resonator. The higher the Q-factor values, the smaller the minimum detectable resonance shift is.

1.2.2 Parallel coupled microring resonators with different ring size

Recent theoretical and experimental investigations have shown that parallel coupled microring resonators exhibit coherent effects similar to those observed in atoms, where electromagnetically induced transparency occurs as a result of quantum interference effects in a coherently driven atom with an external radiation [9]. Unlike the atom-radiation system, where the initial state of the system and the amplitude of the pump are the determining factors, the induced transparency in coupled resonators is controlled by the geometry of the structure.

The input light coming from the source will pass directly to the output port if the two rings are out of resonance. If only one of the rings is at resonance, the light from the source coupled to this ring passes through the drop port. Thus, the transmission spectrum shows a dip like a single ring resonator system.

On the other hand, if both rings are at resonance, the input light will not be coupled directly to the second waveguide. Rather, for an optimum center-to-center distance between the rings, the light from the source is coupled to the second ring. In this case, the two rings act like a mirror reflecting the light from one waveguide to the other between the two rings [9]. Thus, light is coupled into both ring resonators and they form a Fabry-Perot (FP)-like cavity with light traveling in the direction of the arrows indicated in Figure 1-3 below.

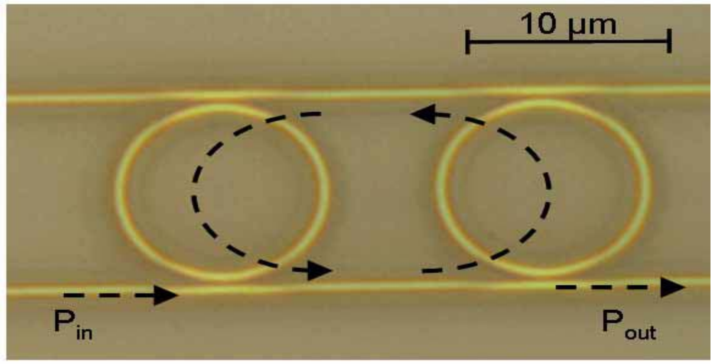

Figure 1-3 Picture of a parallel coupled microring resonator taken from Ref [10]

Theoretically the power transmission of coupled ring resonators is given by [9]

$$|T(\lambda)|^2 = \left(\frac{|t_1 t_2|}{1-|r_1 r_2|}\right)^2 \frac{1}{1+4\left(\frac{\sqrt{r_1 r_2}}{1-|r_1 r_2|}\right)\sin^2\theta}, \qquad (1.4a)$$

Where t_1 and t_2 are complex transmission coefficients for resonator 1 and 2 and are given by

$$t_{12} = \frac{j(\omega-\omega_{12})+\gamma}{j(\omega-\omega_{12})+\gamma+\gamma_c} \qquad (1.4b)$$

$r_1$and $r_2$the complex reflection coefficients, given by

$$r_{12} = \frac{\gamma_c}{j(\omega-\omega_{12})+(\gamma+\gamma_c)} \qquad (1.4c)$$

with ω_{12} is the resonance frequency of resonator 1 or 2, ω is the frequency of the input light , $\gamma = \pi c/Q_{rad}\lambda_0$ is the amplitude radiative-loss rate related to the radiative quality factor, $\gamma_c = \pi c/Q_c\lambda_0$ is the total waveguide-ring amplitude-coupling rate due to decay, $\theta = \frac{1}{2}Arg[r_1 r_2 e^{-2j\beta(\omega)s}]$ is one-half the round-trip phase accumulated in the waveguide, s is the center-to-center distance between the rings, and $\beta(\omega)$ is the waveguide dispersion relation [9]. Note that Q_{rad} and Q_c are the radiative and coupling quality factors for each ring, respectively

Experimental and simulation results revealed that the transmission spectrum of a parallel coupled ring resonator exhibits a very narrow transparency peak in a relatively broader transmission dip for a proper choice of CTC distance between the rings and the detuning between the ring resonances.

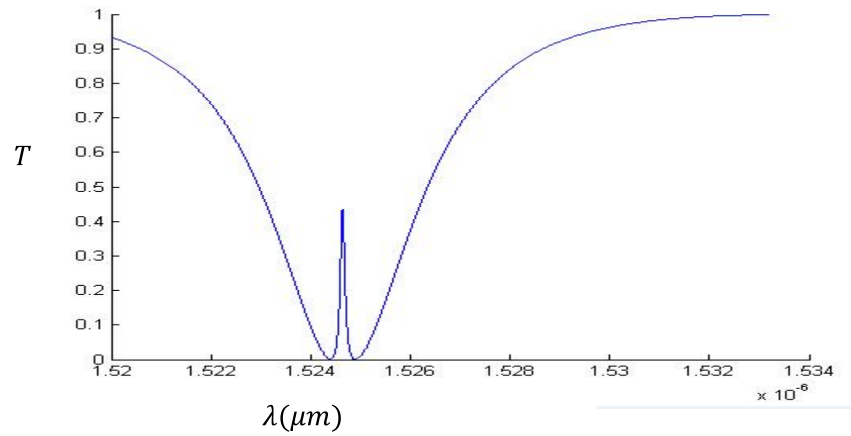

Figure 1-4 Transmission spectrum simulated for s=15.69μm, Δλ=0.4nm, Q_c=1000, and Q_{rad}=25000

For such a symmetrical narrow resonance peak to exist one should leave a slight difference in the size of the rings to detune the ring resonances by a very small amount so that the FP- mode will appear exactly between the resonance modes of the two rings, and the CTC distance between the rings should be properly adjusted. Later on we will see how these parameters affect the position, the width, and the overall nature of the transmission peak. It is worth mentioning that the remarkable narrow peak for the optimum CTC ring separation is a signature for the coherent resonant interaction between the two rings [9].

1.2.3 Parallel coupled microring resonator with same ring size

The transmission spectrum for parallel coupled ring resonators with the same ring size is slightly different from those with different ring size resonators discussed in the previous section. Simulation results showed that, at resonance, the FP-resonance mode will be either to the right or to the left of the common resonance mode or disappear otherwise.

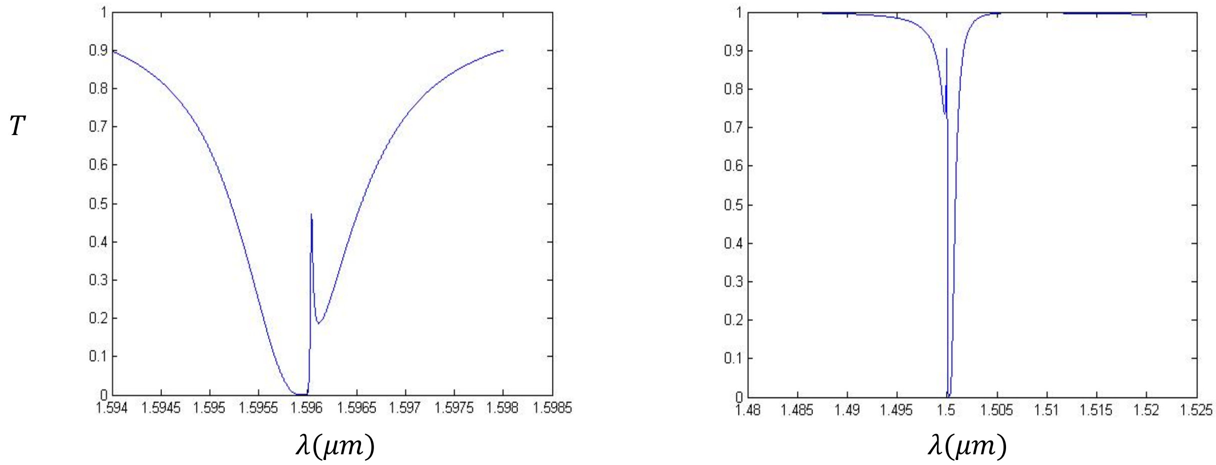

Figure 1-5 Simulation result of Power transmission for parallel coupled ring resonators with size R=5um

The asymmetric nature of the transmission peak for a parallel coupled ring resonator with the same ring size seems to be a problem to examine and compare its performance with other filter configurations since the width of the peak needs to be redefined in some way. Nevertheless, the peak width of these resonators is found to be smaller than those with different ring sizes at a specific height defined for this purpose.

1.3 Basic Principles of Biosensing Based on SOI Microring Resonators

For common sensing applications such as bio/chemical sensing, the interaction between molecules and sensing layer leads to change in refractive index in the layer. Consequently, the light mode supported by the ring resonator experiences this change through its evanescent field, leading to change in effective index [2]. This, in turn, results in shift in resonance wavelength of the mode. Employing equation (1), in general, the shift in resonant wavelength with effective index and physical dimension change is given by:

$$\frac{\Delta\lambda}{\lambda} = \frac{\Delta n_{eff}}{n_{eff}} + \frac{\Delta L}{L} \tag{1.5}$$

The first contribution for the shift in resonance is the change in n_{eff} which actually changes when the refractive index on the surface of the ring is modified by the interaction of analytes with sensing layer. Any mechanical effect leading to the change in the size of the ring structure could also modify the optical mode in the resonator and hence leading to a shift in the resonance wavelength. However, this does not apply to our structure, thus the second term on the right side of the above equation can be ignored.

Light repeatedly circulates at the surface of the dielectric microring structure, increasing the effective length of interaction between light and the sample. The effective interaction length is proportional to the quality factor; therefore, one has to carefully design a micro ring structure with a relatively high Q-value to lower the detection limit. This can be achieved by minimizing the possible losses from scattering and radiation due to bending.

1.4 General Idea of the Thesis

A parallel coupled ring resonator filter configuration in SOI has been studied and compared with a channel-drop filter configuration in terms of their performance for biosensing and bulk refractive index change detection. The effect of relative size of the rings, in a coupled ring resonator systems, on their transmission property has also been investigated through simulation. It has been found that a small detuning in resonance wavelength is essential to achieve a very narrow symmetrical transmission peak. In order to obtain a very sensitive sensor, we have to make sure that not only the spectral shift is large, but also the dips in the spectrum are narrow so that very small shifts can be detected. To this end, the CTC separation between the rings and the coupling coefficients are optimized for a better performance of the filter.

In this thesis, parallel coupled ring resonator structures are fabricated using CMOS facilities at IMEC, Leuven. The structures are patterned on SOI wafer using 193nm deep UV optical lithography. This lithography technique gives better control over feature sizes of the structures. The structures are then formed by etching 220nm thick top Silicon layer on the wafer. The silicon layer is buffered from the substrate by 2μm thick bottom SiO_2 cladding. These SOI coupled ring resonators are designed to operate in telecom wavelength range.

Chapter Two

2. Design

2.1 Theoretical Background of Optical Waveguides and Design

In general, a waveguide is a physical structure that has the ability to guide and confine energy in the electromagnetic spectrum. Waveguides that operate in the visible or IR portion of the spectrum include fiber optics used in telecommunication, as well as micro-fabricated ridge or rectangular waveguides on thin films such as SOI. Both of these waveguide platforms rely on a dielectric guiding medium called the core of the waveguide, surrounded by a lower index material called the cladding. The propagation of an electromagnetic field through such a structure can be easily understood by the use of the ray optics model described by Snell's Law [13].

$$n_1 \sin \theta_1 = n_2 \sin \theta_2 \tag{2.1}$$

Another way of understanding the concept of TIR and the behavior of a reflected wave is through Fresnel's equations describing the reflection coefficient. The reflection coefficient is a multiplier that relates the amplitude of the incident electric field (E_i) on a dielectric interface to the amplitude of the reflected field (E_r).

Directing an electromagnetic wave through such structures utilizes the concept of total internal reflection(TIR), the reflection that occurs when light, in higher refractive index medium, strikes an interface with a medium having a lower refractive index at an angle of incidence(with respect to the normal) satisfying a certain condition. The simplest structure that can be understood by this method is the slab waveguide [14].

If n_1, n_2, and θ_1 are correctly chosen it is possible for θ_2 to become 90°, a condition often termed as total internal reflection, where the incident light impinging on the interface is reflected back into the first medium. The point at which the incident angle θ_1 allows for this condition is called the critical angle and is calculated to be $\theta_c = \sin^{-1}(n_2 / n_1)$. A waveguide structure works in such a way that each interface reflection occurs at an angle larger than θ_c as a result the light ray will theoretically continue in the core region indefinitely.

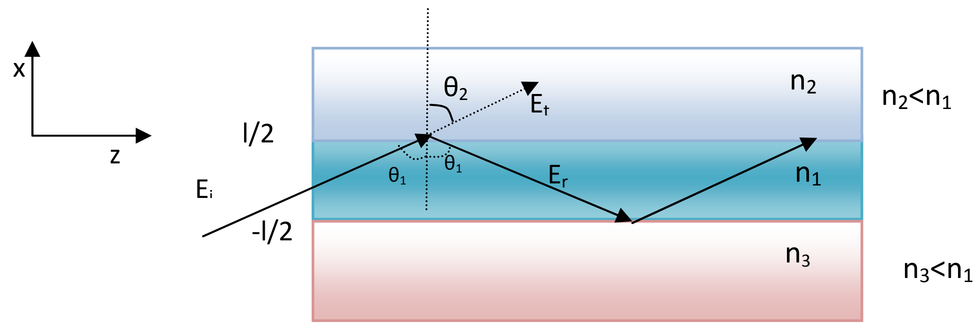

Figure 2-1 Schematic diagram of an asymmetric slab waveguide

Figure 2.1 shows a typical example of a slab waveguide. It consists of a thin dielectric layer acting as a core sandwitched between two semi-infinite bounding media or claddings. It should be noted that the index of refraction of the core must be greater than those of the surrounding media. Moreover, the thickness of the core or the guiding layer is typically on the order of a wavelength. In general, the upper and lower cladding layers can be different and thus termed as an asymmetric slab waveguide. If the two layers are identical it is said to be symmetric.

However, such systems are simply mathematical models often analyzed to understand real systems that are much more complicated in terms of their dimension, inhomogeneity, and other parameters if taken in to account. Analytical solutions for the guided modes of real systems are very difficult and hence one has to look for numerical solutions.

To analyze real systems numerically, one of the most efficient software used to simulate and solve modes of a propagating electromagnetic wave is FIMMWAVE. It is designed to model a wide variety of 2D and 3D waveguide structures using a rigorous fully vectorial formalism. The program is based on a fully vectorial waveguide solver employing the film mode matching method. The vector mode solver will locate almost any horizontal or vertical mode order of arbitrary or mixed polarization. The method is in general substantially faster and more accurate than finite element or finite difference methods [15].

In this thesis, we designed a waveguide using FIMMWAVE for both the straight and curved section in SOI with a 450nm wide and 220nm thick silicon core (n_1=3.4) on top of SiO_2 (n_3=1.5) with water as a top cladding (n_1=1.33). Having all these parameters, the symmetric and antisymmetric guided quasi TE-modes of the coupler, with a gap about 180nm between the waveguides, have been solved and found to be:

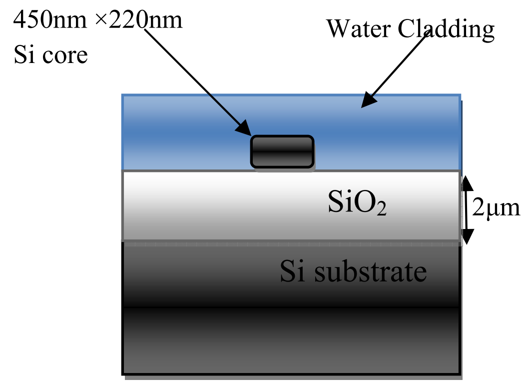

Figure 2-2 waveguide structure in SOI

$$\beta_{+}=\frac{2\pi}{\lambda}n_{+} \qquad (2.3a)$$

and

$$\beta_{-}=\frac{2\pi}{\lambda}n_{-}, \qquad (2.3b)$$

respectively, where n_{+} =2.34434 and n_{-} = 2.311768 with λ=1.5 μm.

2.2 Coupler Design

The ring resonator structures discussed in the first chapter are special cases where the input from the source is coupled to the ring at a point and are sometimes referred to as lumped ring resonators. In such resonators, the coupling can only be controlled by the gap (g) between the bus and the ring. Another ring structure that allows a great control over the amount of coupled light to the ring is called racetrack resonator structure shown in Figure 2-3 where a straight segment is included between the two curved sections acting as a coupler.

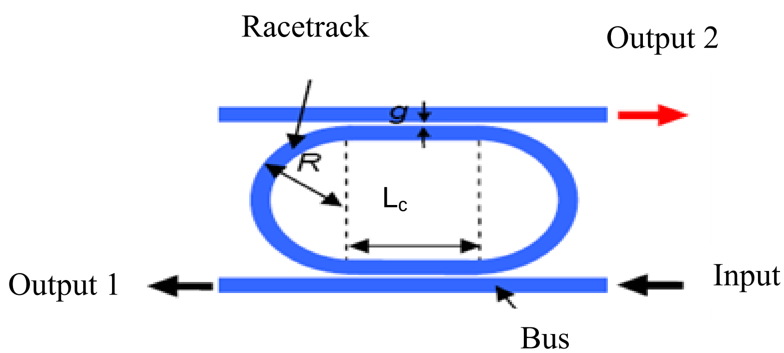

Figure 2-3 Schematic diagram of a racetrack shaped ring resonator

An advantage of racetrack resonator is to design large coupling efficiency with a relatively longer coupling length when even the gap is reasonably wider. The size of such ring structures, however, increases slightly as compared to rings without coupler and hence the waveguide loss increases accordingly. As we can see in Figure 2-3, the racetrack resonator consists of two curved and two straight waveguides forming four different junction points. At resonance, the input light coupled to the racetrack will propagate both in the curved and the straight waveguides and also encounters an interface at the four junction points. The dominant propagation loss in the straight sections of the race track is predominantly due to surface roughness scattering at the sidewalls of the waveguide, which has been extensively investigated [16]. Propagation loss in the curved waveguide sections of the racetrack is due to both bending loss and surface roughness scattering. However, due to the high degree of field confinement in the high-index contrast waveguides, it is expected that the loss due to bending to be very small.

The main loss mechanism in the curved sections of the racetrack, thus, comes also from scattering due to sidewall roughness. The curved waveguide loss is found to increase with the bending radius because the total length of the curved sections becomes larger, although the distributed scattering loss decreases with the radius of the curved waveguide.

Finally, the loss due to modal mismatch at the junctions between straight and curved waveguides is considerable especially when the bending radius of racetrack is very small. It has been observed that [16], for racetracks with large bending radii, surface-roughness scattering in the curved sections produces the biggest loss. As the bending radius decreases, the modal mismatch at the junctions between straight and curved waveguides becomes the dominant loss mechanism.

Because the round-trip propagation loss in small-radius racetrack microresonators is dominated by modal mismatch at the junctions between straight and curved sections, one can reduce the resonator loss by minimizing the junction losses. This can be achieved by introducing an optimum lateral offset between the straight and curved waveguides [16].
In addition, the FSR is inversely proportional to the size of the racetrack or any ring structure and thus one should take such parameters into account to optimize the size of the coupler.

Power is coupled between the modes of two parallel waveguides separated by a finite distance if there is a physical overlap of the mode wavefunctions. Exchange of power between guided modes of adjacent waveguides is well known as directional coupling.

The power transfer between two waveguides, in particular from the input waveguide to the straight section of the racetrack as a function of the propagation distance (z), coupling coefficient (C), and phase mismatch (δ) is given by [14]

$$P_2(z) = P_0 \frac{C^2}{C^2+\delta^2} \sin^2\left(\sqrt{C^2+\delta^2}\right) z \qquad (2.4)$$

where P_0 is the input power coming from the source through the bus wave guide and $P_2(z)$ is the power through the straight segment of the racetrack at a distance z. We note that complete power transfer occurs in a distance $L = \pi/2C$ provided that the phase mismatch between the two waveguide modes, δ, is zero. If there is a non-zero phase mismatch between the two modes, the maximum fraction of power that can be transferred to the second waveguide is found to be $\frac{C^2}{C^2+\delta^2}$. We note that the Q-factor value of our device associated with the coupling loss for each ring is taken to be 1000 to relax on the possible fabrication errors. To this end, 30% of the total power has to be coupled to our coupled ring resonator structure.

We have, therefore, determined the length of the coupler that is long enough to couple 30% of the input power assuming a lossless waveguide and a complete phase matching between the modes. In this case, the ratio of the power coupled to the racetrack with a coupler length of L_c is given by:

$$\frac{P(z=L_c)}{P_0} = 1 - \tau^2 = \sin^2(\mathrm{C}L_c) \qquad (2.5)$$

where C is the coupling constant between the symmetric and antisymmetric supermodes in the two waveguide in terms of their propagation constant given according to Equations (2.3a) and (2.3b) and is found to be:

$$C = \frac{\beta_{+} - \beta_{-}}{2} = 0.066\mu m^{-1} \tag{2.6}$$

Substituting the value $\tau = \cos(CL_c)$ into Equation (1.3), one can reach at

$$(Q_c\lambda)\sin(CL_c)\tan(CL_c) = 2\pi L n_g \tag{2.7}$$

For small values of (CL_c), we can take $\sin(CL_c) = \tan(CL_c) = CL_c$, therefore, Equation (2.7) reduces to

$$Q_c\lambda(CL_c)^2 = 2\pi L n_g \tag{2.8}$$

where, the half round trip is given in terms of the coupler length and the radius of the ring as $L = \pi R + L_c$. Upon substituting this value and rearranging the equation, we obtain

$$L_c^2 - \left[\frac{2\pi n_g}{Q_c\lambda C^2}\right] L_c - \left[\frac{2\pi^2 n_g R}{Q_c\lambda C^2}\right] = 0 \tag{2.9}$$

Equation (2.9) has the form of a quadratic equation in the length of the coupler: $x = ax^2 + bx + c$, with a general solution $x = \frac{-b \pm \sqrt{b^2-4ac}}{2a}$. Solving for L_c, one can show that the coupler length is given according to the equation:

$$L_c = \frac{\pi n_g}{Q_c\lambda C^2}\left[1 \pm \sqrt{1 + \frac{2RQ_c\lambda C^2}{n_g}}\right] \tag{2.10}$$

where the solution with the minus sign should be ignored since the length of any structure cannot assume a negative value. This is one of the quantities we have determined for the completeness of the mask design for our coupled ring resonator structure. In the next chapter we will have a closer look at this and other optimizing parameters.

2.3 ASPIC and Matlab Simulation Results

In this section, simulations for some properties of the three ring resonator structures specifically a single ring resonator, a parallel coupled ring resonator with identical, and with different ring sizes are discussed using a software abbreviated as ASPIC which stands for Advanced Simulation for

Photonic and Integrated Circuit. It possesses a powerful CAD board that permits to construct every circuit starting from the building blocks available in its library, without any restriction in dimensions and complexity. The simulation of the circuit is carried out in the spectral domain and it is many orders of magnitude faster than an electromagnetic simulator, as it uses the scattering matrix formalism. The input/output spectral behavior of the circuit is returned in terms of amplitude, phase, group delay, dispersion and state of polarization. One of the great advantages is that many sources can be defined at the same time and located virtually everywhere, each one with a desired spectral shape, and every point of the circuit is an accessible output port after just only one simulation. ASPIC is based on models collected in Libraries. Depending on the complexity of the implemented models, ASPIC can be used for several purposes [17].

In this thesis, we used ASPIC and Matlab to study the sensitivity and the influence of the CTC distance between the rings and the coupling ratio, C, on the 3dB width of the transmission peak in a coupled ring resonator structure and compare its performance with a single ring resonator. We have also studied the effect of the relative ring size difference in a coupled ring resonator on the property of its transmission.

2.3.1 Optimization Parameters

The basic structure we have considered is a parallel coupled ring resonator on SOI platform. The SOI structure has silicon waveguide of thickness 220nm buffered from the substrate by a 2 µm thick lower SiO_2 cladding.

In order to utilize the change in refractive index for the purpose of biosensing, some structural considerations, particularly the CTC distance between the rings, the length of the coupler, and the overall size of the rings are essential. Qianfan Xu etal and our simulation and experimental results have confirmed that the CTC distance between the rings strongly affects the symmetry and the width of the power transmission peak of the structure. We note that the CTC distance is directly related to the phase accumulated by the travelling electromagnetic wave in between the two rings (the round trip phase shift) which in turn highly affects the transmission spectrum of the device.

The following figures show this phenomenon and are simulated using Matlab and employing the formula for the transmission of a parallel coupled ring resonator given in Equation (1.4a). The Q-factor corresponding to coupling loss is taken to be 1000, and 25000 is taken for the value of the Q-factor corresponding to the radiation loss.

A small detuning of 0.4nm in the resonance wavelength of the individual rings has been adopted from previous works [9] assuming that it is small enough to produce the desired narrow and symmetric peak for our research purpose.

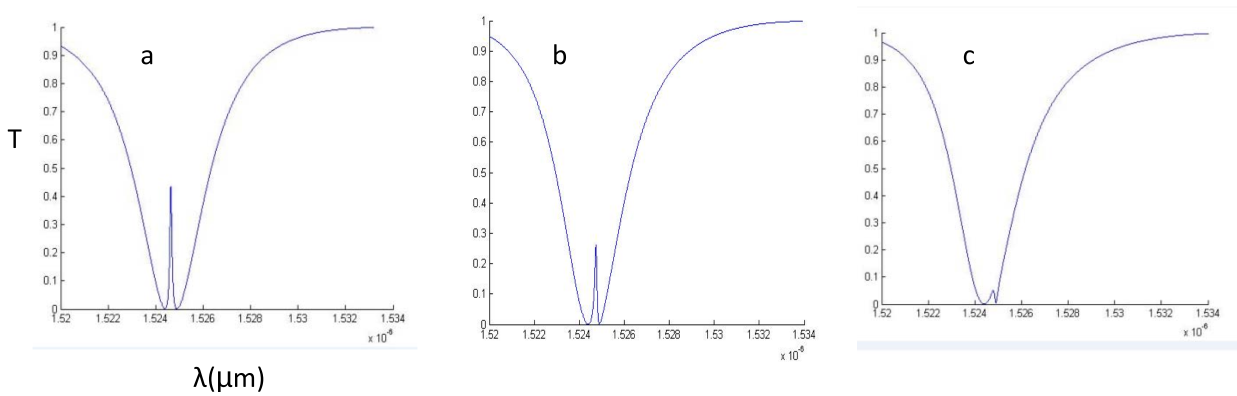

Figure 2-4 Transmission of parallel coupled ring resonator a) for S=12.69um, b) for S=12.71um, c) for S=12.73um

The results shown in Figure 2-4 revealed that the CTC distance between the rings in a coupled ring resonator has a significant influence on the width of the transmission peak and the symmetry of the overall transmission spectrum as the spacing between the two mirrors of a Fabry-Perot cavity determines the transmission spectrum. Hence, it is one of the parameters optimized for the best performance of our structure.

The coupling and propagation losses are directly related to the Q-factor of a resonant system which, in turn, has a significant influence on the detection limit of the sensor. As we pointed out in the first chapter, as the resonance becomes narrower, the resolution improves because it is easier to measure small changes in the reflected/transmitted wavelength peak. The narrowness of the resonant peak is mathematically related to the Q-factor as $Q = \lambda_0/\Delta\lambda$ for a resonator. Here, λ_0 is the center wavelength of the resonance, and $\Delta\lambda$ is the spectral width of the resonance determined at one half of the peak maximum [12].

Therefore, we have also optimized the coupling ratio, κ, for the best performance of our structure in terms of the detection limit. In the next sections, simulation results are discussed for the three ring resonator structures studying their sensitivity and detection limit as well.

2.3.1.1 ASPIC simulation results for the sensitivity of ring resonators

Sensitivity is another figure of merit of a biosensor which is the measure of how much the resonance wavelength of the resonator shifts for a given change in the effective refractive index felt by the field expanding from the core to the upper cladding. We have simulated the sensitivity of both a coupled ring resonator with the same and different ring size and compared their performances with a single ring resonator.

In this simulation, the radius of each ring is taken to be 5µm for all ring resonator structures except a small size difference about 8nm is taken to achieve a detuning value of 0.4nm between the resonance wavelengths of the two rings for the coupled ring resonators with different size. Moreover, the CTC distance between the rings is taken to be 12.45µm which corresponds to the minimum distance set between them in our mask design. The coupling ratio, κ^2=0.3, is taken assuming the Q-factor corresponding to coupling loss to be 1000 for each ring.

When propagation loss is considered in both the straight and curved waveguides, the transmission decreases by a certain amount but the sensitivity is unaffected. This may be due to the fact that the sensitivity of biosensors based on refractive index change is independent of the intensity that is coupled to the ring or transmitted through the pass port. Rather, it depends on how far the evanescent field extends to the cladding and interacts with the surrounding. Considering a propagation loss about 2.4dB/cm, a redshift of 0.5nm has been obtained for a refractive index change of about 10^{-3} RIU which corresponds to an effective refractive index sensitivity of 500nm/RIU. Figure 2-5 shows the drop spectrum and the corresponding redshift graph of a single ring resonator.

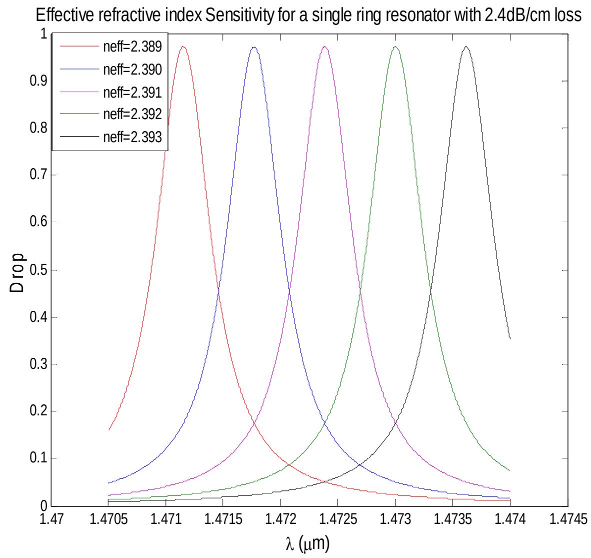

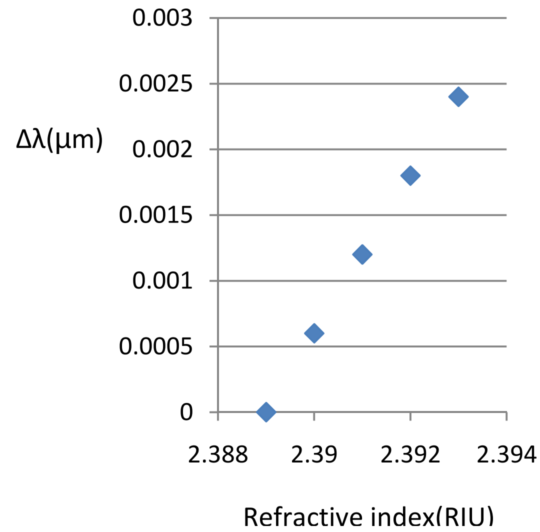

Figure 2-5 ASPIC simulation result (left) for the transmission spectrum (right) for the sensitivity of a single resonator with loss

2.3.1.2 ASPIC Simulation results for the sensitivity of a parallel coupled ring resonator with identical and different ring size

As we discussed in the first chapter, the peak of the transmission spectrum of a parallel coupled ring resonator with the same ring size lies either to the left or to the right of the common resonance position and disappear in some cases. In a lossless case and with the CTC distance between the rings taken, the transmission becomes almost unity and when the refractive index changes, the resonance wavelength shifts. We obtain an effective refractive index sensitivity of 500nm/RIU which is similar to the single ring resonator case considered previously.

The transmission spectrum of a parallel coupled ring resonator with different ring size has a transmission peak positioned between the resonance wavelengths of the individual rings although it can disappear, broaden, or shift for some values of the CTC distance between the rings as shown in Figure 2.4 and the amount of loss considered. A strange result we obtained here is that the transmission peak of the resonator doesn't approach to one even if the propagation loss is ignored. This shows that in the case of coupled ring resonators, the transmission is not only affected by the possible losses but the distance between the rings is also an important parameter to be considered. Therefore, the reason for this phenomenon could be the CTC distance between the rings we chose gives the maximum transmission only that we obtained in Figure 2 that is about 60%. The redshift due to the increment in the value of the effective refractive index is similar to other ring structures considered above.

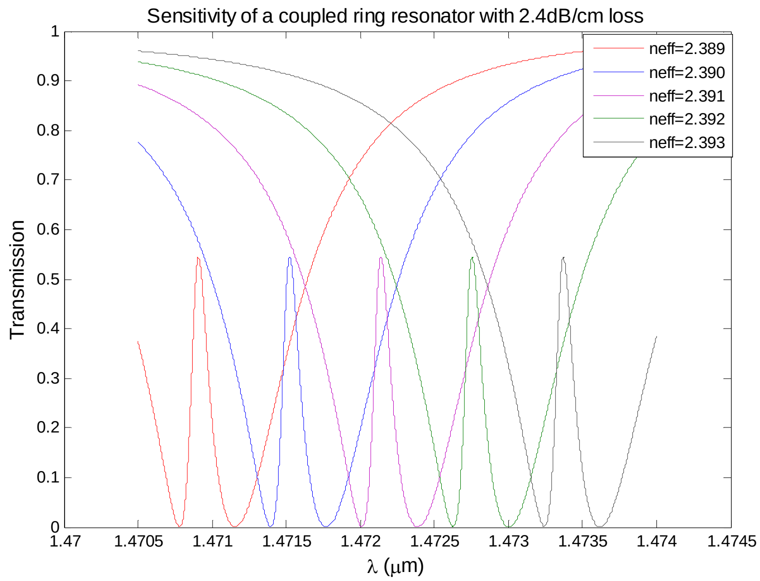

Figure 2-6 ASPIC simulation result for the sensitivity of a parallel coupled ring resonator with different ring size and without loss.

The sensitivity is the same as we obtained in the lossless case and also with other ring resonator structures. The transmission peak decreases by small amount due to the loss we considered.

From the simulation results obtained above, we see that the shift in resonance wavelength is almost independent of the propagation loss attributed to the waveguides. In addition, this shift is almost the same for the three ring structures considered. This is actually due to the fact that the resonance wavelengths of the individual rings shift by the same amount for the coupled ring resonators having the same or different ring sizes. Thus, it gives the same performance as in the case of a single ring resonator in terms of sensitivity. We have also shown that the transmission peak of a coupled ring resonator could be below the expected value without the presence of loss depending on the distance between the two rings.

2.3.2 Influence of the device parameters on the peak width

In the previous section, we have described the sensitivity of the three ring resonator structures considered both in the presence and absence of propagation losses. It should be noted that the performance of a biosensor is measured not only by the amount of shift that the resonance wavelength of the filter undergoes when the refractive index of the surrounding changes, but also the spectral width of the resonance at one half of the peak maximum (FWHM), determines how good our device is performing for the specified purpose since it determines the smallest resonance wavelength shift one can detect, and thus determines the smallest amount of biomolecules that the sensor can detect.

Sensitivity refers to the magnitude of sensor response to a given change in surface adsorbed mass density or refractive index, and detection limit refers to the smallest change in mass density or refractive index that can be measured. It is an especially critical performance criterion for detection of analyte present at low concentration or detection of adsorbed molecules with low molecular weight [5].

In view of this, we simulated the full width at half maximum of the transmission peak for the three ring resonator structures and compared their performance in terms of the ability to detect as small change in refractive index as possible.

Figure 2.7 shows the full width at half maximum (FWHM) of the three ring resonator structures as a function of the coupling ratio. The CTC distance between the rings of the two coupled ring resonators is taken to be 12.45µm which corresponds to the smallest distance in our real fabricated devices. As we discussed in the previous sections, the coupling ratio is chosen as an optimizing parameter because it is directly related to the Q-factor and hence with the FWHM.

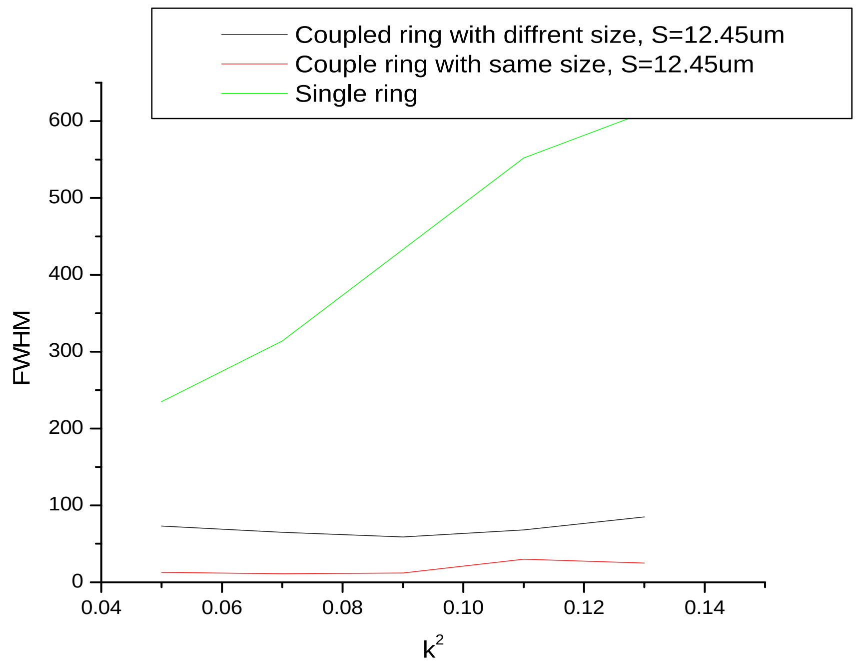

Figure 2-7 FWHM swept over the coupling ratio

As we can see from Figure 2.7 above, the FWHM of a single ring resonator is almost by an order of magnitude greater than that of the two coupled ring resonator structures. This shows that one advantage of our ring resonator structure over a single ring resonator is having a relatively lower detection limit and hence enables us to detect smaller environmental changes than we do using a single ring resonator. Comparison of the performance of a coupled ring resonator having different ring size with that of the resonator having the same ring size shows that a coupled ring resonator with the same ring size performs relatively better. However, the asymmetric nature of the resonance transmission spectrum makes it inconvenient to measure its FWHM.

After observing the significant influence of the coupling ratio and the CTC distance between the two rings in a coupled ring resonator structures, simulations have been done in Matlab for different values of these parameters to determine an optimum region for the best performance of our devices for both the same and different ring size cases. Figure 2.8 shows the simulation result obtained for a coupled ring resonator with detuning between the resonance wavelengths about 0.4nm.

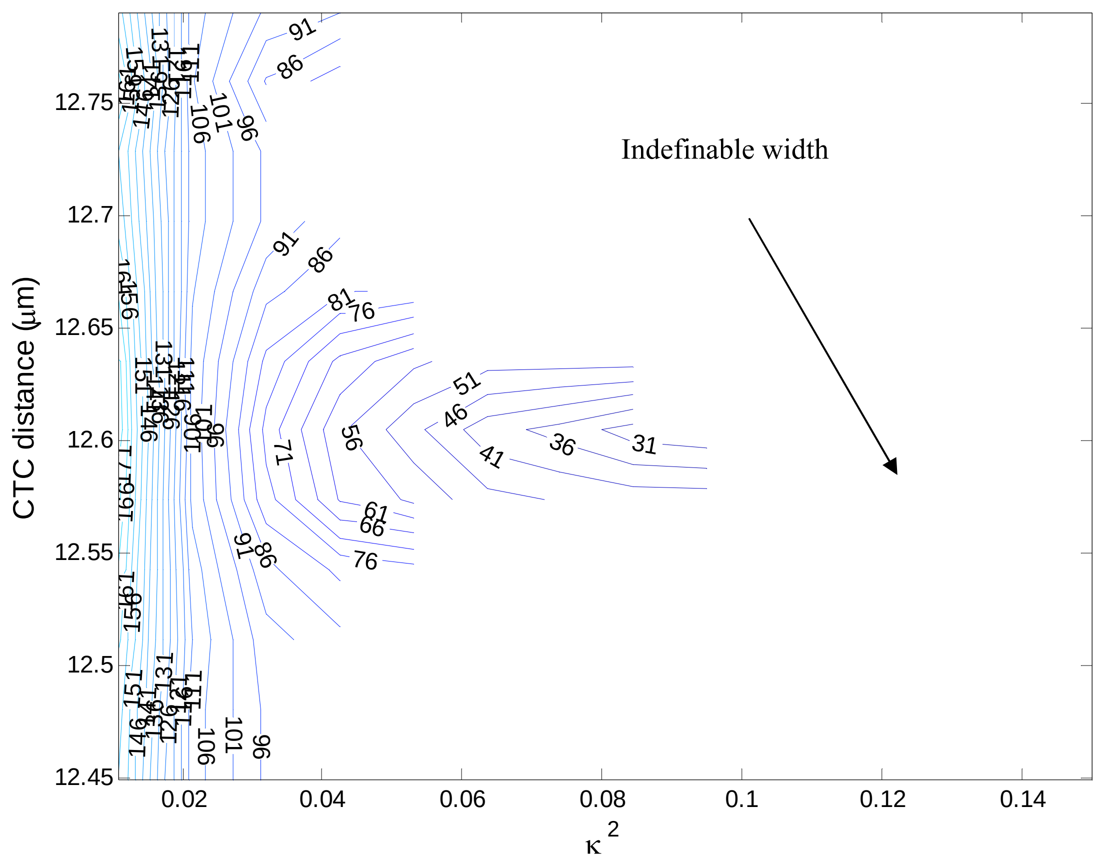

Figure 2-8 Full width at 90% of the transmission peak of a coupled ring resonator with detuning 0.4nm swept over the coupling ratio and the CTC distance betwen the rings.

The values of the full width are in picometers (10^{-12}m) and are taken at the 90% of the transmission peak to make a fair comparison with that of the same size coupled ring resonator. As we pointed out in the previous sections, the transmission spectrum of a coupled ring resonator with the same ring size is not symmetrical with respect to the position of the peak and is therefore impossible to define the full width at half maximum at least in some cases as shown in Figure 2-9.

As we can see from Figure 2-8, the width of the transmission spectrum has got an optimum value about 31pm for the CTC values between 12.6 µm and 12.65µm and for the values of the coupling ratio between 0.08 and 0.09.

The simulation result of the full width for the transmission peak of a parallel coupled ring resonator with the same ring size, defined at 90% of the peak, is shown in Figure 2-9.

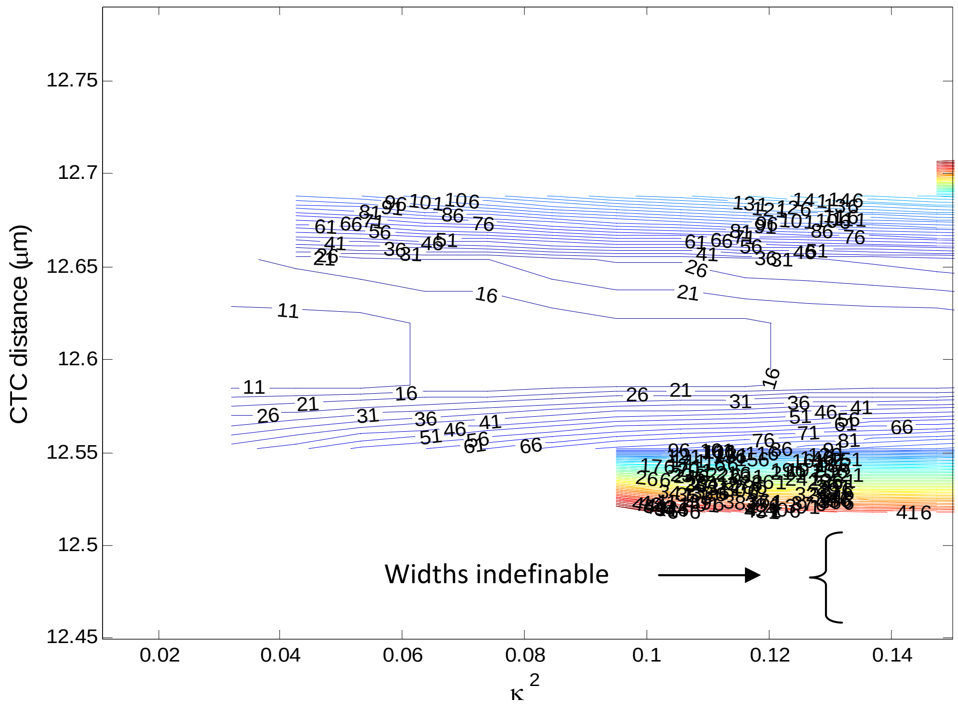

Figure 2-9 FW at 90% of the transmission peak for a coupled ring resonator with the same ring size swept over the coupling ratio and the CTC distance betwen the rings.

As in the previous case, the full width at the 90% of transmission peak for a coupled ring resonator with the same ring size has an optimum value about 11pm for the values of the CTC around 12.6μm and the value of the coupling ratio between 0.04 and 0.08. We note that the colored regions indicate regions of very high widths and the regions indicated by an arrow (inset) are regions of indefinable widths either due to less developed or no peaks at all. Comparison of the results obtained in both cases (Figure 2-8 and Figure 2-9) shows that coupled ring resonators with the same ring size can provide relatively narrower width than that of the ring resonator structures with different size. Nevertheless, the asymmetric nature of their resonance spectrum could be a drawback.

2.3.3 Summary of the chapter

FIMMWAVE has been used to simulate and solve the symmetric and antisymmetric propagating modes of a coupler formed by 450nm×220nm silicon core waveguides with an optimum gap 180nm and water cladding in SOI platform. The coupling coefficient of these modes has been determined and used to calculate the length of the coupler for a maximum of 30% power transfer to the ring waveguides.

The two figures of merit of a biosensor, sensitivity and detection limit, have been discussed in detail. Simulation results have shown that the sensitivity of the three ring resonator structures are almost the same and are independent of the propagation loss in both the straight and curved waveguides considered. However, comparison of the value of the FWHM of the transmission spectrum for the three structures has shown that a coupled ring resonator based biosensor with the same or different ring size can perform better than that based on a single ring resonator since its FWHM is less almost by an order of magnitude.

Finally, taking the asymmetric nature of the transmission spectrum of a coupled ring resonator with the same ring size into account, the full width at the 90% transmission peak has been defined and optimized with the CTC distance between the rings and the power coupling ratio. Matlab simulation results confirmed that there exists an optimum region for this parameter for the values of the CTC distance around 12.6μm and the coupling ratio between 0.08 and 0.09 for the coupled ring resonator with different ring size and between 0.04 and 0.08 with the same ring size. For this particular simulation, an optimum full width at the 90% transmission peak value of 31pm has been obtained for the coupled ring resonator structure with different size and 11pm with the same ring size.

Chapter Three

3. Fabrication and Measurement results

In this chapter, the mask design and the fabrication processes are briefly discussed. Experimental results are presented and compared with the simulation results obtained in the previous chapter.

3.1 Mask Design

The first step towards the fabrication of a photonic or electronic integrated circuit is to design the mask layout so as to imprint the desired patterns on a given substrate. In this thesis, we have used the software called Python including the homemade libraries IPKISS and PICAZZO to design the mask for our structure shown in Figure 3-1. The mask viewer, Clewin, has also been used to view and check whether our design meets the desired criteria.

The design consists of two racetrack shaped rings having bend radius of 5µm. Both the straight and curved waveguides are designed to be 450nm wide and 220nm thick. The gap between the bus and the straight segment of the racetrack is taken to be 180nm. The length of the coupler has been optimized in such a way that 30% of the total power can be coupled to the ring resonator to achieve a Q-factor value of 1000 for each ring resonator. The equation we derived in the previous chapter (Equation 2.9) has been employed to calculate the length of the coupler to transfer the required power to the ring resonators. It has been found that a coupler length of 9.4µm is required for the Q-factor value associated with the coupling loss in each ring assumed to be Q_c=1000. A group index value n_g=3.89, center wavelength λ=1.55 µm, and the value of the ratio of the power coupled to the ring calculated from the corresponding Q-factor are taken.

To investigate the influence of the CTC distance between the rings on the width of the transmission peak, it has been swept in 20 steps from its minimum value S_0=12.45µm to its maximum value S= S_0+Δs=12.774µm, where Δs=0.324µm is a small change in the CTC distance that will result in a phase accumulation of π. This can be shown using the equation:

$$\Delta\theta = \frac{2\pi}{\lambda} n_{eff} \Delta s, \qquad (3.1)$$

with λ =1.55 μm, n_{eff}=2.389, and $\Delta\theta$ being the phase accumulated due to a small change in CTC distance Δs . The minimum distance between the rings, S_0, has been determined considering the size of their radius (2R=10μm), the width of the waveguide (0.45 μm), and the minimum distance between the closest curved waveguides is taken to be 2μm since we are working with a center wavelength of λ =1.55μm which limits the minimum distance between two features during fabrication.

It is worth mentioning that some of the design parameters such as the radius of the rings, the thickness and width of the waveguides, and the minimum distance between the closest curved waveguides have been adopted from previous works.

The overall mask layout consists of a design of twenty such coupled ring resonators each having different CTC distance between the rings as described above.

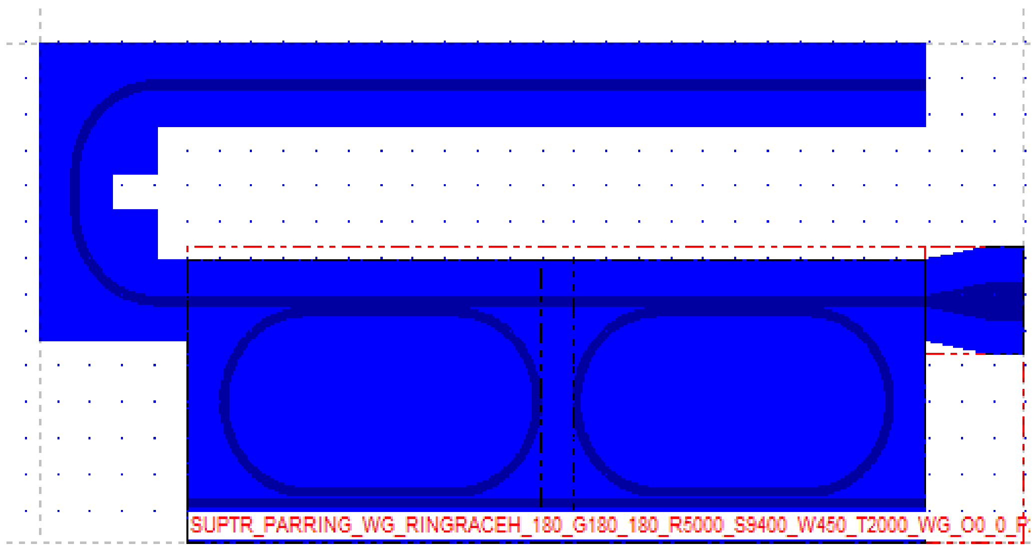

Figure 3-1 Mask design for a coupled ring resonator

We left the size of the rings in each coupled ring resonators the same assuming that there could be achieved about 0.5nm detuning in resonance wavelength from fabrication error. We note that the waveguide on the upper right side is illuminated by a scattered light while it is coupled from the nearby ring to the upper bus [9]. Light does not propagate through that waveguide and tapering has been made to avoid any back reflection from this edge.

3.2 Fabrication

The coupled ring resonator structures described in the previous section for the implementation of biosensors are fabricated using CMOS facilities at IMEC, Leuven. The structures are patterned on SOI wafer using 193nm deep UV optical lithography. This lithography technique gives better control over feature sizes of the structures. The structures are then formed by etching 220nm thick top silicon layer on the wafer. The silicon layer is buffered from the substrate by 2µm thick bottom SiO_2 cladding. These SOI coupled ring resonators are designed to operate in telecom wavelength range.

The fact that our ring structures are fabricated in the SOI platform highly reduces the dimensions of the devices. Due to the high refractive index contrast, the waveguide core is largely reduced in size that will in turn enable to make the waveguide single mode and total internal reflection guiding is assured for very small bend radii. A drawback of the high lateral index contrast is that the waveguides become more sensitive to scattering at roughness on the core cladding interface [18].

For research purposes, nanophotonic devices are usually fabricated using e-beam lithography. Although this is a very precise technique, it is a sequential writing process, making it slow and unsuited for mass fabrication. On the other hand, conventional optical lithography, with illumination wavelengths down to 300 nm, is used for the fabrication of current photonic integrated circuits (ICs) but lacks the resolution to define dense nanophotonic structures like photonic wires. To this end high-quality and high-resolution fabrication tools are required. Deep ultraviolet (UV) lithography, the technology used for advanced complementary metal–oxide–semiconductor (CMOS) fabrication, provides both the required resolution and the throughput needed for commercial applications [3, 19].

The fabrication process with deep UV lithography is similar to that of conventional optical projection lithography. The basic fabrication process steps followed to fabricate our structures are illustrated in Figure 3-2 .First, the photoresist is spin coated on top of the SOI wafer and then prebaked. On top of the photoresist, an antireflective (AR) coating is spun to eliminate reflections at the interface between the air and the photoresist. These reflections could give rise to standing waves in the photoresist, and therefore inhomogeneous illumination. Then, the wafer is sent to the stepper, which illuminates the photoresist with the pattern on the mask. After lithography, the resist goes through a post-exposure bake and is then developed [19].

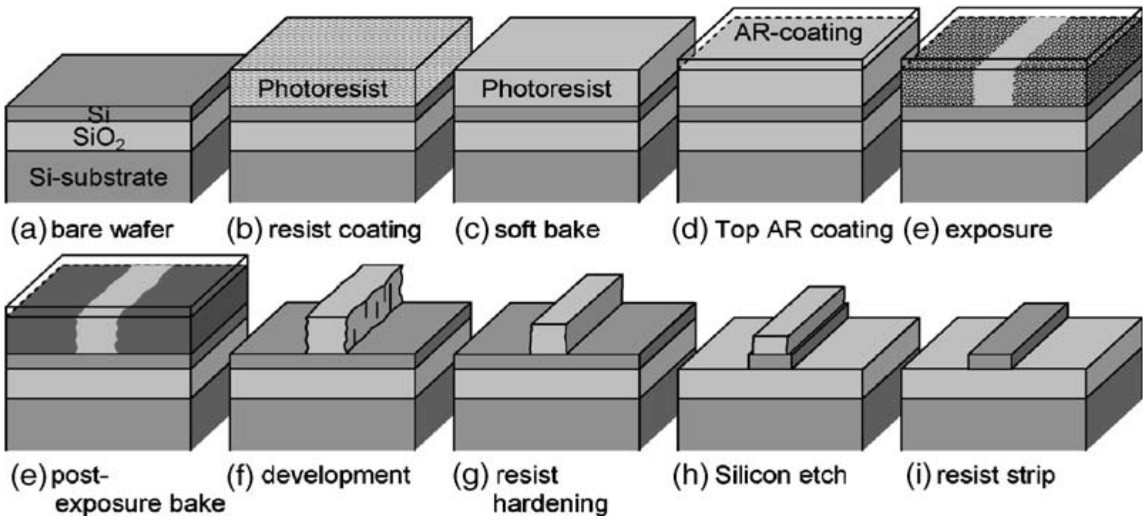

Figure 3-2 Fabrication process for nanophotonic structures in SOI using deep UV lithography [19]

3.3 Measurement

A schematic diagram of the measurement setup is demonstrated in Figure 3-3. Input light from a tunable laser is vertically coupled to the SOI coupled ring structure. The laser has tuning resolution of about 5pm and it is tunable in 1500-1640nm wavelength range. Coupling from optical fiber to the waveguide structures is achieved with grating couplers.

The transmitted or reflected light from our sample is coupled to the output fiber coupler through grating couplers. The output fiber coupler is directly connected to the photodetector so that the reflected or transmitted light through our structure can be measured. To couple light to and from the fiber couplers, one has to optimize its vertical and horizontal position with respect to the grating couplers. Since our structures are highly polarization sensitive, one also has to optimize

the polarization of the input light using the polarization controller shown in Figure 3-3. The measured values are then sent to the computer and scanned in real time using suitable software.
The following figure shows the measurement setup we have used to characterize our structures. We note that only the basic components of the setup are included, others, such as the camera used to visualize our structure and the fiber couplers, are skipped.

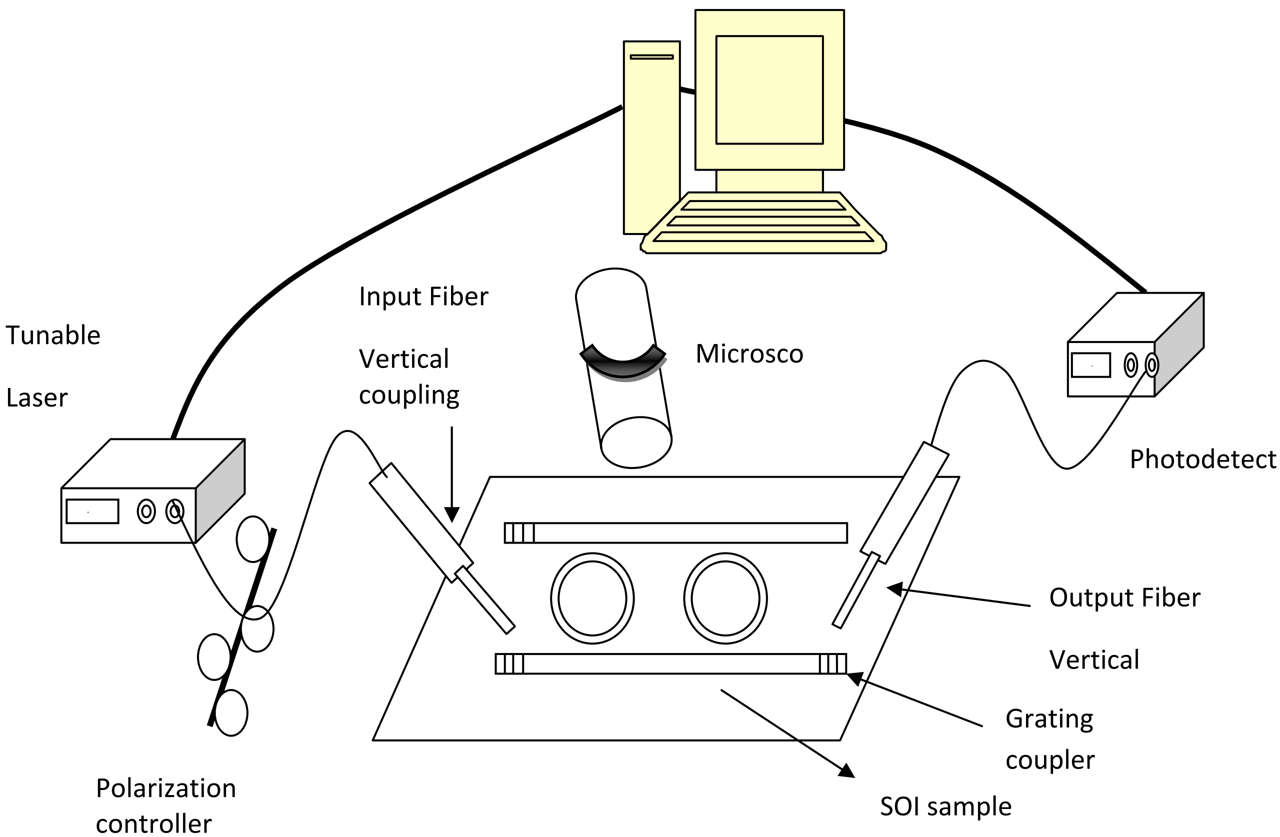

Figure 3-3 Schematic diagram of the measurement setup

The sample to be characterized is seated on a small fixed holder. The fiber couplers are attached with a movable holder so that one can optimize their position for maximum transmission.
After optimizing the position of the fiber couplers and the polarization of the input light for the minimum possible loss, we have measured the transmission spectrum of our samples for both water and air top cladding. We put a drop of water on top of the sample to keep it as wet as possible in case of water cladding measurements.

3.4 Measurement Results and Comparison with Theory

In this section we will analyze the results obtained from our measurement and then compare them with the simulation results obtained in the previous chapter.

3.4.1 Measurement results

We have measured the transmission and drop spectrum of our structures for air and water claddings at different resolutions. The maximum resolution, 5pm, has been used to analyze our data.

In the first part of this section, the transmission or drop spectrum of our samples using water and air cladding are shown and the results are compared with each other. These results are also compared with the simulation results obtained in the previous chapter. Then, we calculate the width of the transmission spectrums measured at the maximum resolution and compare the result with the outcomes we theoretically obtained.

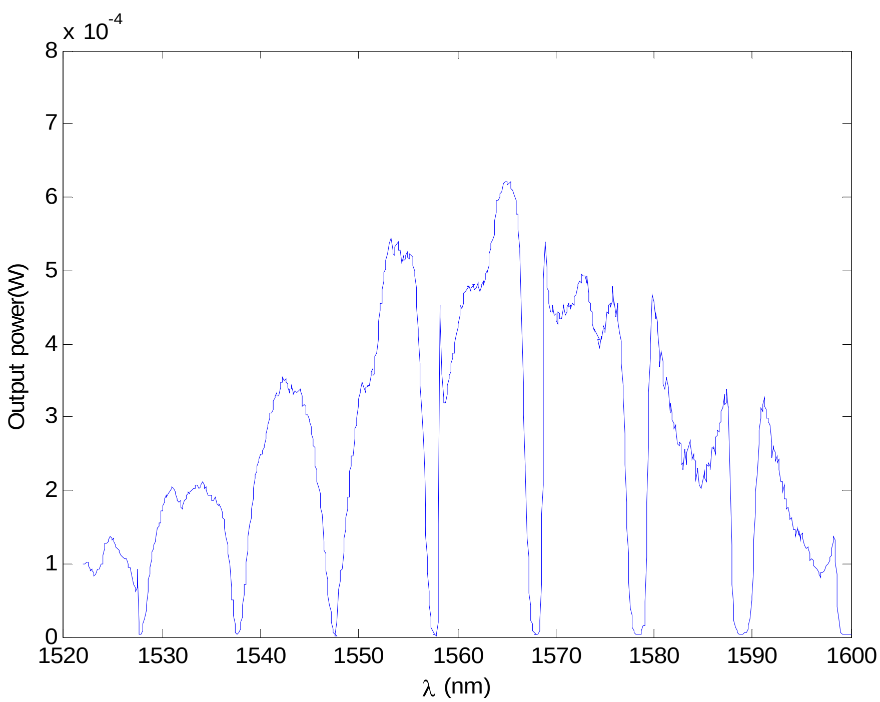

Figure 3-4 Output Power at the pass port with water cladding and CTC distance between rings 12.45μm

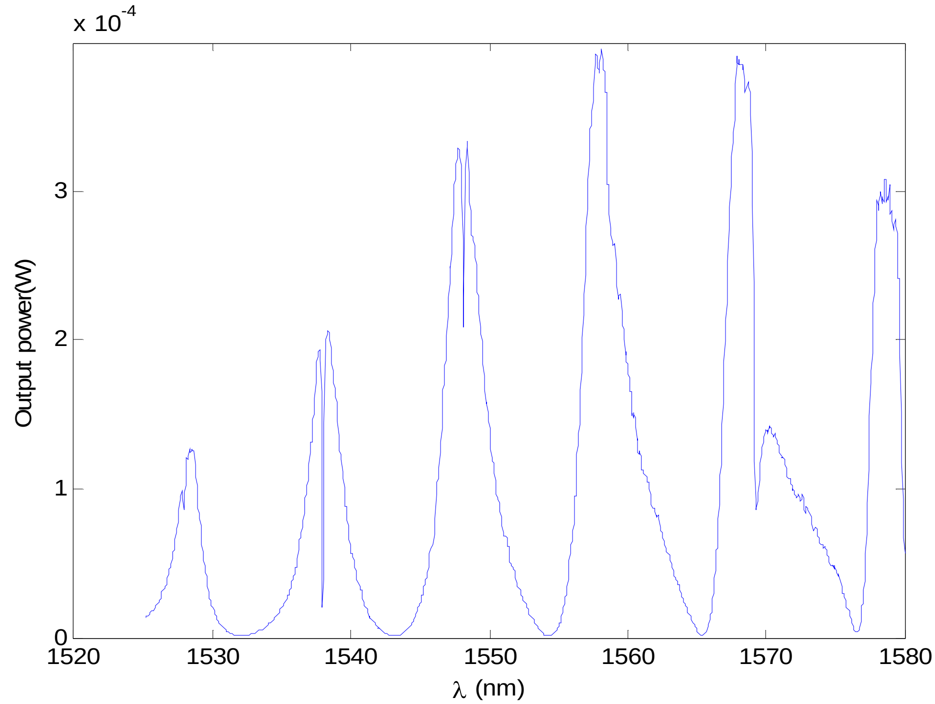

Figure 3-5 Output Power at the drop port with air cladding and CTC distance between rings 12.4824µm

Figures 3-4 and 3-5 show the transmission and drop spectrum of our structures with CTC distance between the rings 12.45µm and 12.4824µm, respectively.

Comparison of these output spectrums with the theoretical results obtained in the previous chapter indicates that some of our samples are fabricated with the same ring size (Figure 1-5 and Figure 3-4) because they have asymmetric transmission peak with respect to the resonance wavelength while some structures are with different ring size (Figure 1-4 and Figure 3-5). Moreover, an induced electromagnetic transparency like transmission, a very narrow peak in the middle of a broader dip, has been realized.

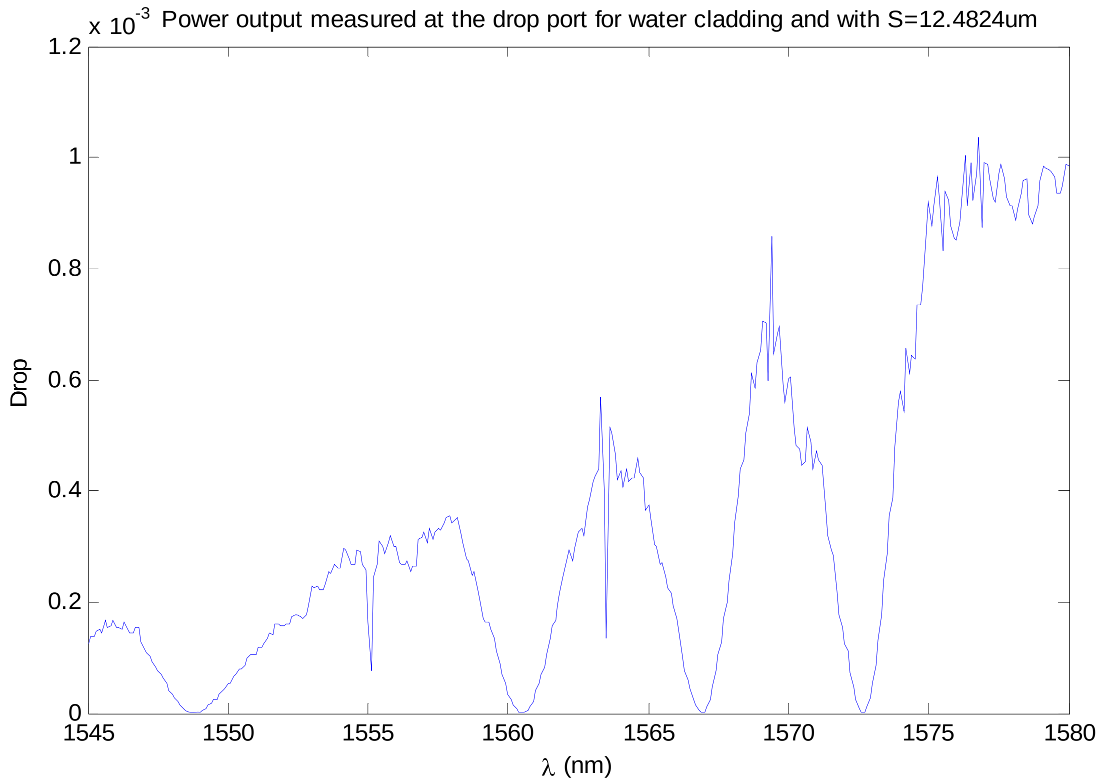

Figure 3-6 Output Power at the drop port with water cladding and CTC distance between rings 12.45µm

Figure 3-6 shows the output power spectrum measured at the drop port with water cladding. Comparison of Figures 3-5 and 3-6 shows that the major resonator dips are much less developed and broader in case of water top cladding. This is actually the pronounced loss due to water absorption.

When we put a drop of water on the sample to keep it as wet as possible, the effective refractive index of the environment will change abruptly and this could be the reason why the spectrum looks noisy.

The widths of the transmission spectrum of the samples at the 90% of the transmission peak have also been calculated for water cladding and compared with the corresponding simulation results for κ^2=0.3. The influence of the CTC distance between the rings on the width of the spectrum is shown in Figure 3-7 below.

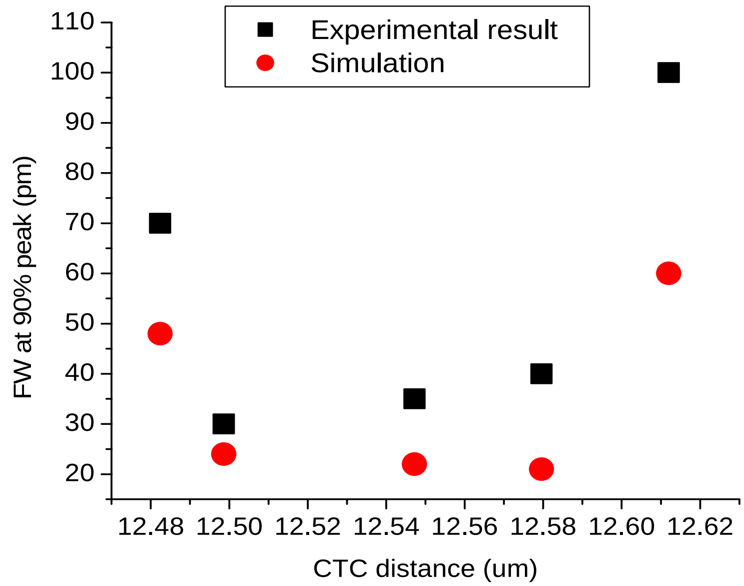

Figure 3-7 Full width at the 90% transmission peak for water cladding and κ^2=0.3

3.4.2 Comparison with theory

The full widths at the 90% of the transmission peak of our samples have been calculated as shown in Figure 3-7. According to the simulation results we obtained in the previous chapter (Figure 2-8), we have seen that there exists an optimum value of the width about 31pm at the 90% peak transmission for the values of CTC around 12.6μm and power coupling ratio between 0.08 and 0.09 if we consider a detuning in resonance of about 0.4nm. Moreover, for a coupled resonator with the same ring size and (Figure 2-9), an optimum full width of 11pm has been obtained for the CTC distance near 12.6μm and 12.65μm and a coupling ratio between 0.04 and 0.08.

Our experimental and simulation results for the performance of our fabricated structures (Figure 3-7) also indicated that there exists an optimum width value at the 90% transmission peak for the values of the CTC distance around 12.5μm and 12.58μm, respectively and with a power coupling ratio assumed to be κ^2=0.3. In this particular simulation, a full width value of 20pm at the 90% transmission peak has been found around the CTC distance indicated. The optimum full width at the 90% transmission peak obtained from our experiment is about 30pm which is a bit higher than the value obtained from our simulation and slightly at a different CTC distance between the rings. This slight deviation from the theoretical result could be due to the pronounced loss form water absorption and misalignment of fiber couplers. Since our structures are highly polarization sensitive, any unnecessary pressure applied on our single mode fibers used could lead to a significant loss. The loss from the fiber connectors should be also taken in to account. Moreover, we believe that the amount of data measured is not large enough to know the exact position and value of the optimum value. Nevertheless, the results obtained from our simulation and experiments are in good agreement.

3.5 Summary of the chapter

In the first part of this chapter, we have briefly discussed about the design of a parallel coupled racetrack shaped ring resonator. In this design, the radius of the racetrack, 5µm, and the dimensions of the waveguide, 450nm×220nm, have been adopted from previous works. Some device parameters such as the CTC distance between the rings and the length of the coupler have been optimized for the best performance of our structure for biosensing purpose. To relax on the possible fabrication errors, we have decided to design our device with a Q-factor value associated with the coupling loss for each ring to be 1000. To this end, 30% of the total power has to be coupled to our ring resonator structure. It has been found that a coupler length of about 9.4µm is necessary to transfer the desired amount of the total power coming from the source to the ring resonator.

The CTC distance between the rings has been swept from its minimum (12.45µm) to its maximum (12.774µm) value in twenty steps so that the value providing the best performance can be determined. Although a very small size difference between the two rings of a coupled ring resonator is essential to obtain a symmetric transmission spectrum with a very narrow peak in the middle of a relatively broader dip, we have left their size the same assuming a detuning in resonance wavelength of about 0.5nm can be achieved from fabrication error. Our measurement results have shown that some of our structures are of the same ring size with asymmetric transmission spectrum and others are with different ring size having symmetric EIT like transmission.

The coupled ring resonator structures described above are fabricated using CMOS technology at IMEC, Leuven. The waveguide structures are patterned on SOI wafer using 193nm deep UV optical lithography. The structures are then formed by etching 220nm thick top silicon layer on the wafer. The silicon layer is buffered from the substrate by 2µm thick bottom SiO_2 cladding. The basic fabrication process flow to fabricate nanophotonic structures has been briefly presented. First, the photoresist is spin coated on top of the SOI wafer and then prebaked, then an antireflective (AR) coating is spun on top of the photoresist. Finally, the wafer is sent to the stepper, which illuminates the photoresist with the pattern on the mask. After lithography, the resist goes through a post-exposure bake and is then developed. Since our structures are fabricated in the SOI platform, their dimensions can be highly reduced and due to the high refractive index contrast, the waveguide core is largely reduced in size which makes the waveguide single mode and total internal reflection guiding guaranteed for very small bend radii.

Finally, the experimental setup to characterize our samples has been shown. Using a tunable laser with maximum resolution down to 5pm as a power source and a photodetector, the transmission spectrum of our samples has been obtained. It has been shown that the transmission spectrum of our devices is identical to the theoretical EIT like transparency with a narrow peak in a relatively broader dip. Calculation of the width at the 90% of the peak transmission has shown that there exists an optimum width value of 30pm for the CTC distance between the rings around 12.5µm assuming the power coupled to our structure is the same as our design, κ^2 =0.3. This is in well agreement with the theoretical result (Figure 3-7) that a coupled ring resonator with resonance detuning of 0.4nm has an optimum full width at 90% of the transmission peak about 20pm for the CTC around 12.58µm and the same power coupling ratio considered.

Chapter Four

4. Summary and recommendations

In this chapter, we summarize the main points discussed in the previous chapters and draw important conclusions. Some future plans and recommendations are also included.

4.1 Summary

A parallel coupled racetrack resonator filter based on the SOI platform has been designed, fabricated, and characterized for biosensing. We have also studied the transmission properties of our device through simulations and compared its performance with a channel-drop filter configuration for the aforementioned purpose.

In general, implementation of biosensors using ring resonators has several advantages over other approaches. The fact that they do not involve a facet or gratings for their optical feedback makes them suited for monolithic integration with other optical devices. In addition, a specific transmission spectrum can be designed by the use of multiple serial or parallel coupled ring resonators.

In a parallel coupled ring resonator system, at resonance, the input light will not be coupled directly to the second waveguide as it does in a single ring resonator. Instead, for an optimum CTC distance between the rings, the light from the source is coupled to the second ring. Then, the two rings act like a mirror reflecting the light from one waveguide to the other between the two rings. Thus, light is coupled into both ring resonators forming a Fabry-Perot (FP)-like cavity. If the "Fabry-Perot" mode happens to be between the resonance wavelengths of the two rings, a very narrow symmetric transmission peak can be achieved provided that there is a small detuning between the resonance wavelengths of the two rings. Such symmetric and narrow transmission peaks are crucial for the implementation of effective refractive index change for biosensing purpose. Because, as the width of the transmission peak becomes narrower, it is easier to measure small changes in the reflected/transmitted wavelength peak.

One of the figures of merit for a biosensor is its detection limit or its ability to detect as small a shift in resonance wavelength as possible. In view of this, some device parameters that are assumed to have a remarkable influence on the width of the transmission peak have been optimized.

One of the device parameters having a great control over the width of the transmission peak is found to be the CTC distance between the two rings as the spacing between the two mirrors of a Fabry-Perot cavity affects the width and the overall properties of the transmission spectrum. In addition, the power ratio coupled to the ring resonator has an influence on the peak width since it is directly related to the Q-factor of the cavity corresponding to the coupling loss. We, therefore, optimized these parameters for the best performance of our device and compared its performance with the result obtained from an add-drop channel filter configuration.

Simulation results have shown that a parallel coupled ring resonator based biosensor with identical or different ring size can have a lower detection limit relative to a single ring resonator biosensor as it has a FWHM value less by almost an order of magnitude (Figure 2-7) for a properly chosen CTC distance between the rings.

Moreover, a contour plot of the full width at the 90% peak transmission of a coupled ring resonator with different ring size (Figure 2-8) has shown that there exists an optimum value of about 31pm for the values of the CTC between 12.6μm and 12.65μm and the power coupling ratio values between 0.08 and 0.09. For identical ring size coupled ring resonator (Figure 2-9), an optimum value of 11pm has been found for the CTC values around 12.6μm and the values of the coupling ratio between 0.04 and 0.08.

The other figure of merit of a biosensor is its sensitivity which evaluates the response of the device for a given change in the effective refractive index of the environment. In other words, it is the measure of ‘’how much’’ the resonance wavelength of the resonator shifts for a given change in the effective refractive index felt by the field expanding from the core to the upper cladding. Our simulation results confirmed that the sensitivity of a coupled ring resonator with different or the same ring size is the same as a single ring resonator both in the absence or presence of waveguide loss. It has been found that both the coupled and single ring resonator structures have an effective refractive index sensitivity of about 500nm/RIU. This is actually due to the fact that the resonance wavelengths of the two rings of a coupled ring resonator shift by the same amount for a given effective refractive index change and hence the overall shift will be the same as the shift obtained by a single ring.

In addition to the numerical analysis, we have also designed, fabricated, and characterized the proposed device and compared its performance with the simulation results obtained. In our design, the radius of the racetrack is taken to be 5μm, and the dimensions of the waveguide are 450nm wide and 220nm thick, as optimized from previous works.

To relax on the possible fabrication errors, we have designed our device with a Q-factor value associated with the coupling loss for each ring to be 1000 which means that 30% of the total power has to be coupled to our ring resonator structure. It has been found that a coupler length of about 9.4μm is long enough to couple the desired amount of power from the source to the ring resonator.

The CTC distance between the rings has been swept so that the value with the best performance can be determined. The size of the two rings has been left equal with the assumption that a small detuning in resonances could be achieved. From the transmission spectra of our fabricated devices we measured, we understood that some of our devices are with the same ring size (Figure 1-5 and Figure 3-4) while others are with different size (Figure 1-4 and Figure 3-5) having symmetric transmission spectra.

Our structures have been fabricated using CMOS technology at IMEC, Leuven. The waveguide structures are patterned on SOI wafer using 193nm deep UV optical lithography. The structures are then created by etching the 220nm thick top silicon layer on the wafer. The silicon layer is isolated from the substrate by 2μm thick bottom SiO_2 cladding. Since our structures are formed in the SOI platform, their dimension can be highly miniaturized. Owing to the high refractive index contrast, the waveguide core is largely reduced in size and can be made single mode. In addition, total internal reflection guiding is guaranteed for very small bend radii.

Furthermore, the experimental measurements to characterize our samples have been carried out both for air and water top cladding. It has been revealed that the transmission spectrum of our devices is indeed identical to the theoretical EIT like transparency with a narrow peak in a relatively broader dip. Due to the higher losses, in the case of water cladding, the transmission peaks are found to be broader and less developed than the transmission peaks measured with air cladding.

The widths of the transmission peaks of our sample have been calculated for different values of the CTC distance between the rings. Our measurement results have shown that there exists an optimum value of the full width at the 90% peak transmission about 30pm for the CTC distance between the rings around 12.5μm. This is in good agreement with the theoretical results we have obtained.

4.2 Recommendations and Future plan

At the beginning of this thesis work, we have planned to characterize our structures in terms of their performance in both bulk refractive index change and biomolecular sensing. For the case of bulk refractive index detection, liquids with varying refractive indices, for example water with different sodium chloride concentrations, can be flown across the coupled ring resonator structure. The corresponding resonance wavelength shift can be then measured. In case of biomolecular detection, the well known avidin-biotin binding chemistry can be utilized. When a biotinylated solution is introduced to a surface functionalized with avidin, the molecular binding changes the effective index of the microcavity and gives rise to a shift in its resonant modes. Due to its high affinity constant, the avidin/biotin system gives a very specific and stable interaction and can be taken as a model of biomolecular interaction.

In this thesis, we have not made any experimental characterization for both bulk refractive index change and biomolecular detection due to a shortage of time. We have thus a plan to characterize our samples and compare their performance with that of an add-drop channel filter configuration which has been extensively studied.

In addition, other filter configurations such as a micro-cavity resonator coupled with a Mach-Zehnder interferometer can be also characterized for biosensing since it exhibits a narrow and tunable transmission spectrum.

In case of measurements with water top cladding, a temperature controlling mechanism should be devised since adding a drop of water while the transmission is being measured could change the nature of the spectrum as the effective refractive index will change abruptly.

Although TM modes are lossy, we believe they are suitable for biosensing purpose as they are more evanescent in nature and can feel the environmental change easily. Therefore, working with TM modes may improve the sensitivity of the device.

Bibliography

[1] A. Ramachandran etal, A universal biosensing platform based on optical micro-ring resonators, Biosensors and Bioelectronics, 2008, 23 pp 939–944.

[2] Ayca Yalcin, Optical sensing of biomolecules using microring resonators, IEEE J. Selected topics in Quantum Electronics, 2006,12, pp 148-155

[3] Katrien De Vos etal, Silicon-on-Insulator microring resonator for sensitive and label-free biosensing, Optics Express, 2007, 15, pp 7610-7615

[4] B. E. Little etal, Microring resonator channel dropping filters, J. Lightwave Technology, 1997, 15, pp 998-1005

[5] Brian T. Cunningham, Label-free optical biosensors, 2009, Cambridge University press, pp 2-10

[6] Peter Debackere etal, Surface plasmon interferometer in silicon-on-insulator: novel concept for an integrated biosensor, 2006, Opt. Express, 14, pp 7063-7072

[7] Frank V. and Stephen A, Whispering-gallery-mode biosensing: label free detection down to single molecules, Nature Methods. 2008, 5, 591-596

[8] Katrin Schmitt, Interferometric biosensor based on planar optical waveguide sensor chips for label-free detection of surface bound bioreactions, Biosensors and Bioelectronics, 2007, 22 pp 2591–2597.

[9] Qianfan Xu etal, Experimental realization of an on-chip all-optical analogue to Electromagnetically Induced Transparency, Phys Rev. Lett, 2006, 96, 123901, pp 1-4

[10] Qianfan Xu etal, Direct measurement of tunable optical delays on chip analogue to electromagnetically induced transparency, Opt. Express, 2006, 14, pp 6463-6468

[11] M. K. Chin and S. T. Ho, Design and modeling of waveguide-coupled single-mode microring resonators, J. Lightwave Technology, 1998, 16 pp 1433-1446

[12] Pieter Dumon, Altra-compact integrated optical filters in SOI by means of wafer-scale technology, , 2006-2007, PhD dissertation, Ghent University

[13] Grovind P. Agrawal, Fiber-optic communication systems, 2007, 3rd edition

[14] Amnon Yariv and Pochi Yeh, Optical electronics in modern communications, 2007, 6th edition

[15] FIMMWAVE Manual, version 4.3
[16] Yuichiro Tanushi, Design and fFabrication of racetrack optical ring resonator, Advanced science matter,Hirshima University, Japan
[17] ASPIC Manual, version 2.1
[18] Wim Bogaerts etal, Nanophotonic waveguides in Silicon-on-Insulator fabricated with CMOS technology, J. Lightwave Technology, 2006, 12, pp 411-412
[19] Wim Bogaerts etal, SOI nanophotonic waveguide structures fabricated with deep UV lithography, Photonics and Nanostructures, 2004, pp 81-86
[20] Nebiyu Yadelo, An integrated optical sensors in SOI for detection of hydrogen gas, 2007-2008, MSc thesis, Gent University